Zeitschrift: IABSE publications = Mémoires AIPC = IVBH Abhandlungen
Band: 30 (1970)

Artikel: Calculation of stress in knee joints of rigid steel frames of thin walled section and its application
Autor: Okumura, Toshie / Ishizawa, Naruo
DOI: https://doi.org/10.5169/seals-23595

Calculation of Stress in Knee Joints of Rigid Steel Frames of Thin Walled Section and Its Application

Le calcul des contraintes dans l'assemblage d'angle de portiques en acier à nœuds rigides et parois minces et son application

Spannungsberechnung der dünnwandigen, steifknotigen Rahmenecke und deren Anwendung

TOSHIE OKUMURA
Professor of University of Tokyo, Tokyo, Japan

NARUO ISHIZAWA
Technical Division, Miyaji Iron Works Co., Ltd., Tokyo, Japan

Introduction

Rigid frame construction is employed in many of crossroads in cities, and its dynamic properties are now required to be reexamined. From our past experiences, it is known that the knee joints are in most cases weak points in rigid frame construction. Efforts have been made to pursue the properties of knee joints in designing based on the theory of elastic design, and recently the rigid frame construction has been taken up as an example in which the theory of plastic design can effectively be applied. All these have brought knee joints under examination from new angles. Essential property required of knee joints of rigid frame construction is, in general, the property to correctly transfer bending moment from beam to column, which causes a large shearing stress in the knee joints. Particularly, the web of straight knee joints with thin walled box section is subjected to shearing collapse due to this large shearing stress. Therefore, it will be required to have thorough understanding of such shearing stress and to devise a means to reduce it. Concerning this matter, there have been published some reports on utilization of wide flange steel for columns and beams having I-section. The present authors have confirmed from their actual survey of shearing stress distribution in knee joints of rigid frame construction having box section that it is almost a parabolic distribution, and suggested that the calculation made on the assumption that it is a uniform distribution should be corrected.

In straight knee joints, the stress from the inside flange of a column acts on the inside flange of beam as concentrated load, which causes shear lag, and this shear lag produces stress concentration on flange near the beam web. Due consideration must be paid to the stress distribution determined by the dimensions of the section. Reports so far published are, in many cases, on the study of wide flange steel for columns and beams having I-section. The trouble is that the stress is concentrated on the part of flange or web near the line of intersection of inside corners of column and beam, and that when the section formed by welding is used, the point of stress concentration coincides the point of intersection of welded joint. This may affect the ultimate strength of welded composite section under some conditions. From the viewpoint of welding, box section must be considered to be somewhat different so far as the ultimate strength is concerned.

In this report, the authors explain about the calculation of stress due to shear lag in straight knee joint flanges with box section and the diagrams used in estimating the stress, and mention the application of this theory to other types which differ somewhat from the type described.

Cylindrical columns have come to be more used in recent days in view of the advantages of cylindrical construction. Such problems as shearing stress in cylinders at knee joints and shear lag in beam flanges are no exception to this type. With reference to shearing stress in cylinder at knee joints, a system, in which beam web is inserted into cylinder, has been developed and its advantages have been examined in comparison with the simple system to butt beam web to cylinder. Simplified way of thinking has been presented so that the theory on straight knee joint flanges with box section might be applied to the stress in beam flange at knee joint of cylindrical construction.

A circular arc haunch type has been adopted in knee joints of rigid frame construction for railway bridge piers which are subjected to repeated load. Shearing stress in knee joints is generally lessened in this type as compared with other types. The flange force from column to beam is distributed within the range that the arc projection covers the beam axis, on account of which the effect of shear lag on the straight flange is relatively small. In this type, however, the warping of web and arc flange at knee joint is large, which causes fairly high stress concentration in the proximity of the web of arc flange. This report treats of the calculation of stress in arc flange at arc knee joint with box section and provides the results of the experiments.

1. Straight Knee Joint

This type is in the most popular use. In most cases, square steel is fixedly arranged on the line of intersection of the inside flanges of a column and beam. This arrangement is made to cope with problems related to a possible lowering

of yield strength incident to a steel plate subjected to stress in the direction of its thickness and the rigidity of the flanges on the line of intersection and to look for the effect of stress in column flanges distributed in and acting on beam webs.

The Tokyo Expressway Corporation adopts the design method proposed by the present author for the calculation of knee joints. This method is a revised version of L. S. Beedle's theory with respect to shearing stress in webs at knee joints. As regards stress in flanges, due regard is paid to the stress due to shear lag. It is expressly indicated that the stress due to shear lag in flanges can be obtained by model calculation and diagrams used for estimating the stress due to shear lag are presented with the aim of simplifying the calculation.

1.1. Shearing Stress in Webs

Prof. Beedle has published the valuable results of his study on the design of knee joints of rigid frames. He sets forth the advantages of designing knee joints in straight form on the following assumptions:

a) Shearing stress is distributed uniformly in webs.

b) The theory of the maximum shearing stress is observed with respect to yield condition for safety's sake. Therefore, $\tau_y = \sigma_y/2$.

c) Only shearing stress acts on webs, while only normal stress on flanges.

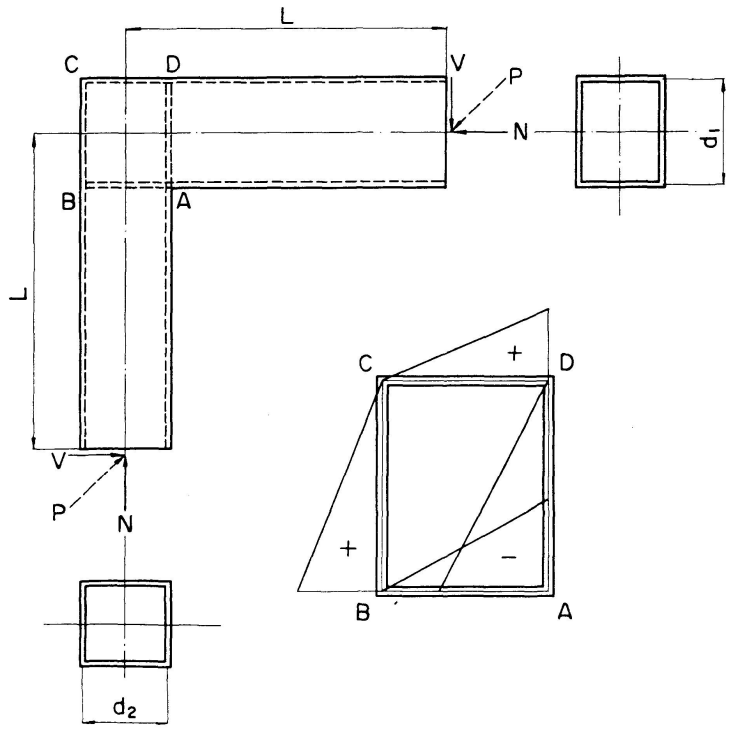

Fig. 1.

According to these assumptions, when members are subjected to loads as shown in Fig. 1, normal stresses in the flanges DC and AB of the beam and the flanges BC and AD of the column attenuate linearly and differences in normal stress are transmitted to their respective webs as shearing stress.

This way facilitates calculation of stress. It is also applicable to straight knee joints of box section.

Let M and N be bending moment and axial force. By referring to Fig. 2, the flange force F can be written in the form

$$F_{01} = \frac{M_1}{d_1} - \frac{N_1}{2}, \quad F_{i1} = \frac{M_1}{d_1} + \frac{N_1}{2}, \quad F_{02} = \frac{M_2}{d_2} - \frac{N_2}{2}, \quad F_{i2} = \frac{M_2}{d_2} + \frac{N_2}{2}. \tag{1}$$

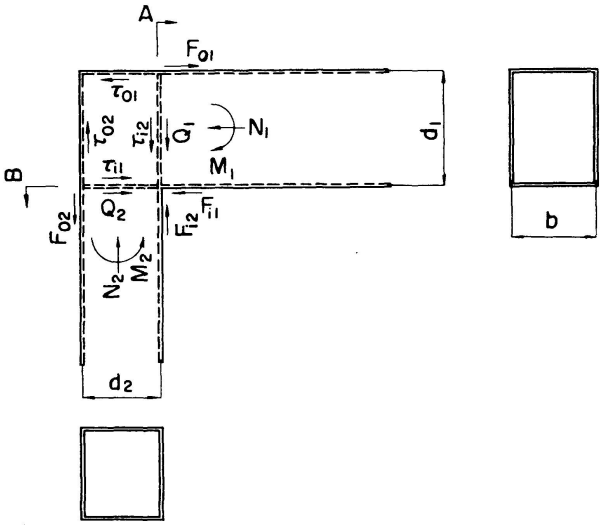

Fig. 2.

Let Q be shearing force, and the shearing stress τ can be written in the form

$$\tau_{01} = \frac{F_{01}}{2d_2t_2}, \quad \tau_{i1} = \frac{F_{i1} - Q_2}{2d_2t_2} = \tau_{01}, \quad \tau_{02} = \frac{F_{02}}{2d_1t_2}, \quad \tau_{i2} = \frac{F_{i2} - Q_1}{2d_1t_2} = \tau_{02}, \tag{2}$$

By referring to Fig. 1, the bending moment at which the webs are caused to yield by shearing stress may be obtained in the form

$$M_{h(\tau)} = \frac{t_2 d_1 d_2 \sigma_y}{2}\left[\frac{1}{1 - \frac{d_1 + d_2}{2L}}\right]. \tag{3a}$$

The bending moment at which the flanges are caused to yield by normal stress is defined as

$$M_{h(\sigma)} = \frac{\sigma_y}{\frac{1 - \frac{d}{2L}}{S} + \frac{1}{AL}}, \tag{3b}$$

where S and A denote the modulus of section and sectional area of the member which is smaller in web height, respectively, and d is the web height of the other member.

Let τ_a be allowable shearing unit stress in Eq. (2) for τ.

$$\tau_{01} = \tau_{i1} \leqq \tau_a,$$

$$\tau_{02} = \tau_{i2} \leqq \tau_a.$$

And τ_a is assumed to be related to allowable tensile unit stress σ_a in the form

$$\tau_a = 0.45\,\sigma_a. \tag{4}$$

The ratio of allowable shearing unit stress to allowable tensile unit stress is estimated at a lower value than that in other parts of bridges in due consideration of the difference between the shearing stress distributed in knee joints assumed in Eq. (2) and that actually observed. It is assumed in Eq. (2) that shearing stress is distributed uniformly in the webs at a knee joint, while, according to the results of actual observations, shearing stress has a somewhat larger value at the middle of the knee joint and near the point of intersection of the inner flanges. In other words, it is disributed approximately in parabolic form rather than uniformly. When the relation between a load and a change in the interval between load points is viewed from the results of experiments, the condition of initial yield is more definitely expressed by the theory in support of the parabolic distribution of shearing stress. By applying $\tau_{av}/\tau_{max} \fallingdotseq 0.9$ (where τ_{max} is the maximum value of the shearing stress assumed to be distributed in parabolic form and τ_{av} is the value of the shearing stress assumed to be distributed uniformly in an ordinary section) to the yield condition $\tau = 0.5\,\sigma_y$ based on the theory of the maximum shearing stress, $\tau_a = 0.45\,\sigma_a$ was proposed for the calculation in which shearing stress is assumed to be distributed uniformly.

Webs tend to become thicker according to this method of calculation than according to conventional methods of calculation. This means a less tendency to stress concentration in flanges due to shear lag. That is to say, welded flanges and webs intersect at one point in three directions in a straight knee joint of box section and the maximum stress is exerted on this point of intersection. In this type, about 1.5 to 3 stress concentration brought about at this point leaves a defect coupled with the quality of welded joints. This knee joint is subject to repeated alternate stress under vehicle and earthquake loads. As the mean stress in this type of knee joint has been allowed to come down to the proximity of the yield point of steel under designed earthquake load, it is subject to high stress low cycle fatigue according to the degree of stress concentration coupled with residual stress due to welding. This is why stress concentration at this part is desired to be reduced to a minimum in some way or other.

1.2. Calculation of Shear Lag Arising in Flanges at Knee Joints and Diagrams Used for Estimating Stress Due to Shear Lag

The problem taken up in designing thin walled section is the phenomenon of shear lag arising in flanges and webs near concentrated load. The phenomenon of shear lag is caused by inner constraint when there is a difference in shearing strain between adjoining sections in the longitudinal direction of flanges. As the stress due to shear lag generally has the same sign as the stress due to bending moment, it comes into question at that part of a member which is subjected to the maximum bending moment. It should be corrected to bending stress to which the law pertaining to the retention of plane can be applied.

Shear lag is analyzed on the following assumptions:

1. Beams have uniform sectional form and are made of a uniform and isotropical elastic body.
2. The flanges are joined to the web at right angle to each other.
3. Bernoulli-Euler's assumption holds good in the web plate and the flanges are the plates on which shearing force and normal stress act along the boundary.
4. Strain remains unchanged at that part where the flanges and the web are welded together on the ground of continuity.

This is shown in terms of boundary condition in Fig. 3. This condition is used for solving the Airy's stress function ϕ.

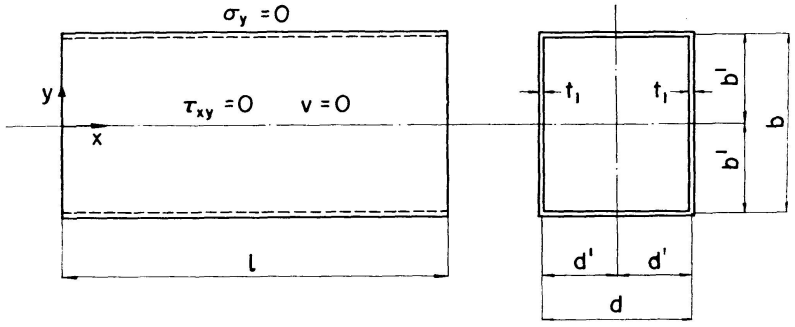

Fig. 3.

From the fact that the strain in the web plate is equal to that in the flanges at $y=b'$ in Fig. 3,

$$\sigma_w = (\sigma_x - \nu\,\sigma_y)_{y=b'} = \left(\frac{\partial^2 \phi}{\partial y^2} - \nu \frac{\partial^2 \phi}{\partial x^2}\right)_{y=b'}. \tag{5}$$

The effective width of the flanges is defined as

$$\bar{b}' = \frac{\int_0^{b'} \sigma_x \, dy}{\sigma_w} = \frac{\left[\frac{\partial \phi}{\partial y}\right]_0^{b'}}{\sigma_w}. \tag{6}$$

The modulus of section S can be written in the form

$$S = \frac{12A_1A_2 + 4A_w(A_1+A_2) + A_w^2}{2A_2 + A_w}\frac{d'}{3} \tag{7}$$

or

$$S = \frac{12A_1A_2 + 4A_w(A_1+A_2) + A_w^2}{2A_1 + A_w}\frac{d'}{3}, \tag{8}$$

where A_w: sectional area of web plate,
$2d'$: height of web plate,
A_1: effective sectional area of upper flange,
A_2: effective sectional area of lower flange.

Hence

$$M = \sigma_w S = \left(\frac{\partial^2\phi}{\partial y^2} - \nu\frac{\partial^2\phi}{\partial x^2}\right)_{y=b'} S. \tag{9}$$

This represents the fourth boundary condition.

By putting

$$M = a\cos(\zeta x + \eta) \tag{10}$$

we obtain

$$\phi = (A\cosh\zeta y + B\sinh\zeta y + C\zeta y\cosh\zeta y + D\zeta y\sinh\zeta y)\cos(\zeta x+\eta). \tag{11}$$

By inserting this in the boundary condition, the effective width $\bar{b}'$ is defined as

$$\bar{b}' = \frac{\cosh\zeta b'\sinh\zeta b' + \zeta b'}{2\zeta\cosh^2\zeta b'} \tag{12}$$

in box section.

Developing the moment acting on the beam into the Fourier series

$$M = \sum_{n=1}^{\infty} a_n \sin\frac{n\pi}{l}x. \tag{13}$$

The stress caused by bending is defined as

$$\sigma = \frac{M}{S} = \sum_{n=1}^{\infty}\frac{a_n}{S}\sin\frac{n\pi}{l}x. \tag{14}$$

When shear lag is taken into account

$$\sigma = \frac{M}{S_n} = \sum_{n=1}^{\infty}\frac{a_n}{S_n}\sin\frac{n\pi}{l}x. \tag{15}$$

Therefore, the stress σ_S due to shear lag can be written in the form

$$\sigma_s = \sum_{n=1}^{\infty}\left(\frac{1}{S_n} - \frac{1}{S}\right)a_n\sin\frac{n\pi}{l}x. \tag{16}$$

The part at which shear lag comes into question in the rigid frame construction is a knee joint. Great shearing force is exerted on the knee joint through which the moment in the column is transmitted to the beam, resulting in shearing deformation and high stress due to shear lag in the section of the knee joint. Moreover, the maximum moment acts on the knee joint, making it necessary to give consideration to the stress due to shear lag.

Let us calculate moment distribution by regarding the variation of shearing force as the concentrated load W applied to the middle of a simple beam.

Developing the moment exerted on the middle of the simple beam into Fourier series

$$M = \sum_{n=1}^{\infty} a_n \sin \frac{n\pi}{l} x.$$

Putting $x = l/2$ in the above equation

$$M = \frac{2Wl}{\pi^2} \sum_{n=1}^{\infty} \frac{1}{n^2}, \qquad (n = 1, 3, 5, 7, \ldots). \tag{17}$$

Hence, the stress due to shear lag in this case is written in the form

$$\sigma_s = \frac{2Wl}{\pi^2} \sum_{n=1}^{\infty} \left(\frac{1}{S_n} - \frac{1}{S}\right) \frac{1}{n^2}, \quad (n = 1, 3, 5, 7, \ldots). \tag{18}$$

Assume that the upper and lower flanges have the same section and let t_1 be the thickness of the flanges, and we can derive from Eq. (7) and (8)

$$S = 4b' t_1 d' + \frac{d'}{3} A_w. \tag{19}$$

Hence

$$\begin{aligned} \left(\frac{1}{S_n} - \frac{1}{S}\right) &= \frac{1}{4b_n' t_1 d' + \frac{d'}{3} A_w} - \frac{1}{4b' t_1 d' + \frac{d'}{3} A_w} \\ &= \frac{3}{A_w d'} \frac{R_S}{1 + R_S} \frac{1 - \frac{b_n'}{b'}}{1 + \frac{b_n'}{b'} R_S}, \end{aligned} \tag{20}$$

where

$$R_S = \frac{6A_f}{A_w} \tag{21}$$

and A_f is the sectional area of each of the upper and lower flanges. Hence

$$\begin{aligned} \sigma_s &= \frac{2Wl}{\pi^2} \sum_{n=1}^{\infty} \frac{3}{A_w d'} \frac{R_S}{1 + R_S} \frac{1 - \frac{b_n'}{b'}}{1 + R_S \frac{b_n'}{b'}} \frac{1}{n^2} \\ &= \frac{Wb'}{A_w d'} \sum_{n=1}^{\infty} \frac{6}{\pi^2} \frac{l}{b'} \frac{R_S}{1 + R_S} \frac{1 - \frac{b_n'}{b'}}{1 + R_S \frac{b_n'}{b'}} \frac{1}{n^2} \\ &= \frac{b'}{d'} \frac{W}{A_w} \boldsymbol{S}_S = \frac{b}{d} \frac{W}{A_w} \boldsymbol{S}_S, \end{aligned} \tag{22}$$

where $$S_S = \sum_{n=1}^{\infty} \frac{6}{\pi^2} \frac{l}{b'} \frac{R_S}{1+R_S} \frac{1-\frac{b'_n}{b'}}{1+R_S\frac{b'_n}{b'}} \frac{1}{n^2}, \quad (n = 1, 3, 5, 7, \ldots). \tag{23}$$

In box section

$$\frac{\bar{b}'_n}{b'} = \frac{\cosh \zeta b' \sinh \zeta b' + \zeta b'}{2 \zeta b' \cosh^2 \zeta b'}, \tag{24}$$

where $$\zeta b' = n\pi \frac{b'}{l}. \tag{25}$$

Therefore, if the value of n is taken far enough, the value of S_S can be calculated accurately. S_S is the function of R_S, $\frac{l}{b'}$ and $\frac{b'_n}{b'}$. Assuming $\frac{l}{b'}=10$, the value of S_S is calculated with respect to all possible values of $R_S=\frac{6A_f}{A_w}$ as shown in Fig. 4. It has been confirmed that, if $\frac{l}{b'}>4$, S_S is little related to $\frac{l}{b'}$.

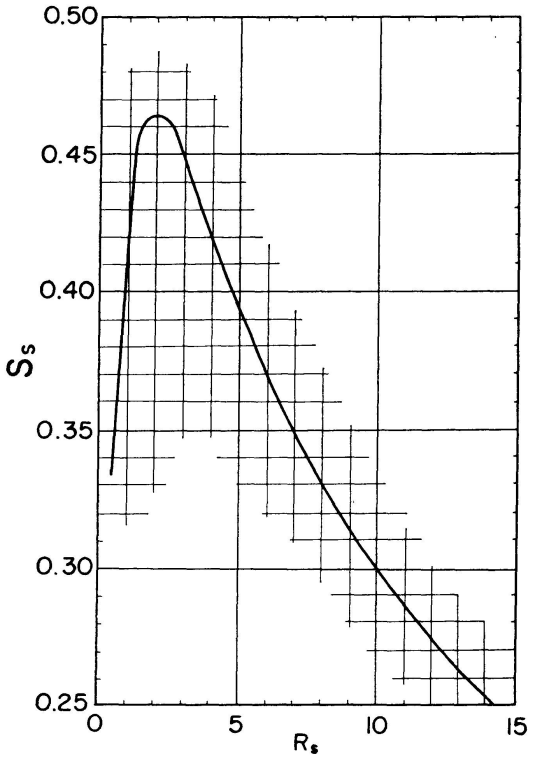

Fig. 4.

Assuming that the web plate of the column transmits no moment and the axial force is only born by the flanges, the inside flange force F_{i2} of the column can be defined as

$$F_{i2} = \frac{M_2}{d_2} + \frac{N_2}{2}.$$

The variation of shearing force in the section AD is defined as

$$W = F_{i2}.$$

If an arbitrary box section is given, we can calculate

$$R_S = \frac{6A_f}{A_w}$$

and find out the value of S_S to R_S by referring to Fig. 4. Therefore, σ_S can be calculated easily from

$$\sigma_S = \frac{b}{d}\frac{F_{i2}}{A_w} S_S. \tag{26}$$

The maximum stress in the flanges can be calculated from the bending stress σ_B and the stress due to axial force σ_N on the assumption that the beam is subjected to pure bending moment.

$$\sigma_{max} = \sigma_B + \sigma_N + \sigma_S. \tag{27}$$

1.3. Results of Experiments

The results of experiments with this type are illustrated as follows.

Fig. 6 shows shearing stress in the webs at the knee joint and Fig. 7 and 8 show axial stress in the flanges.

The results of these experiments indicate that the values obtained by the above-mentioned calculations are very close to the measured values.

An $M - \Delta i$ curve is shown in Fig. 9. Δi is the amount of a change in load

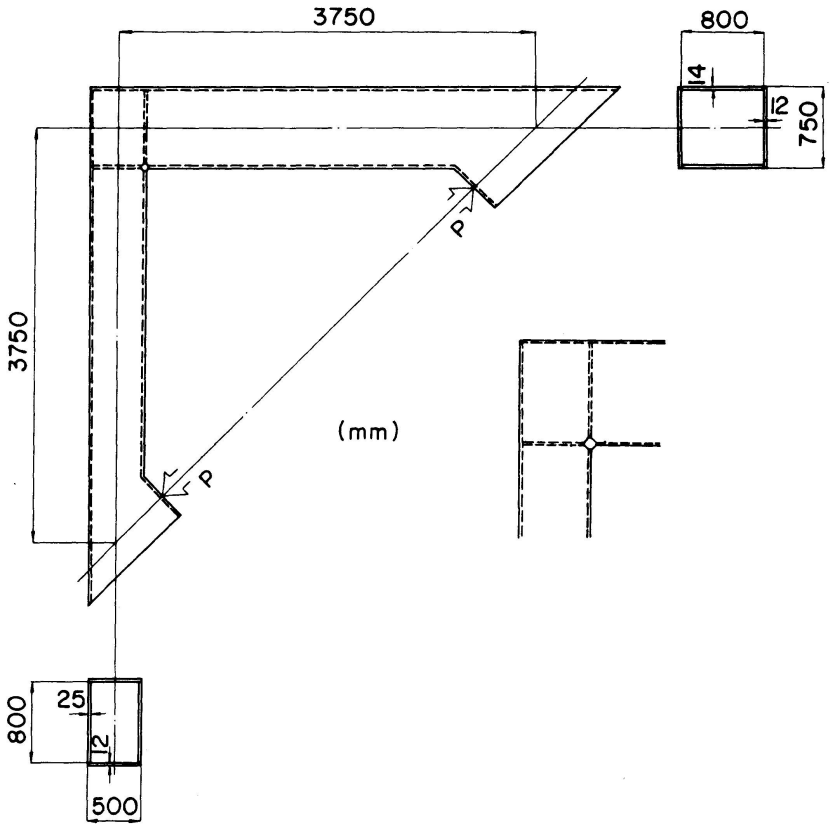

Fig. 5.

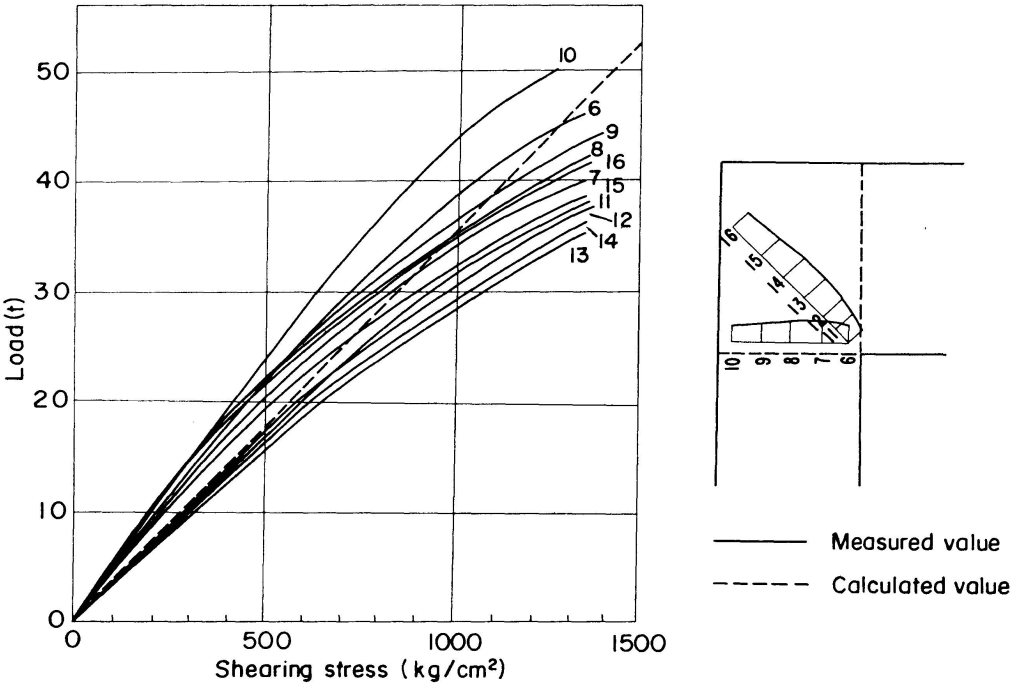

Fig. 6.

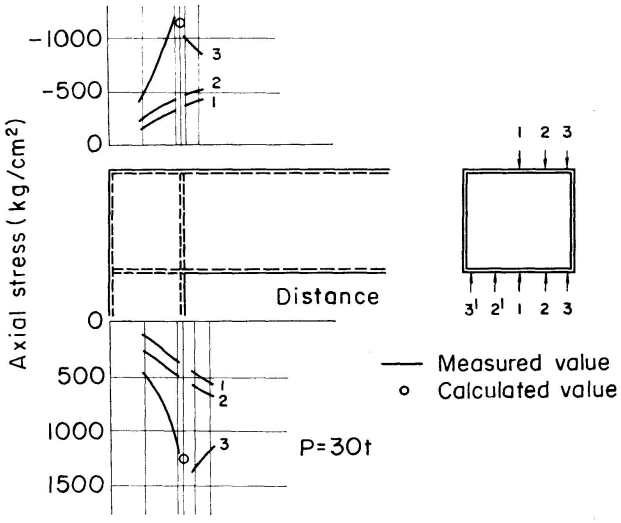

Fig. 7.

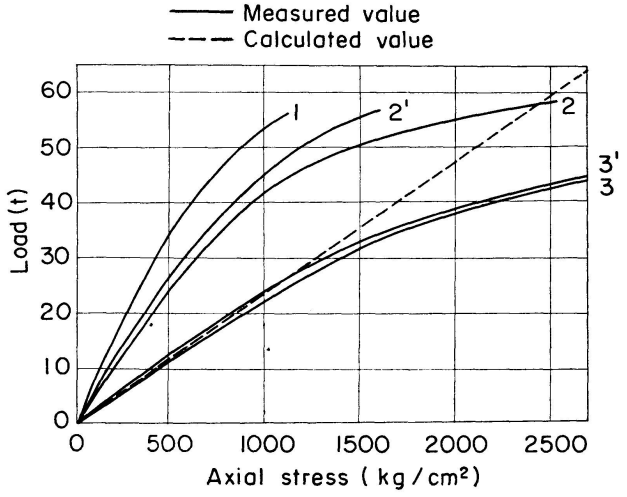

Fig. 8.

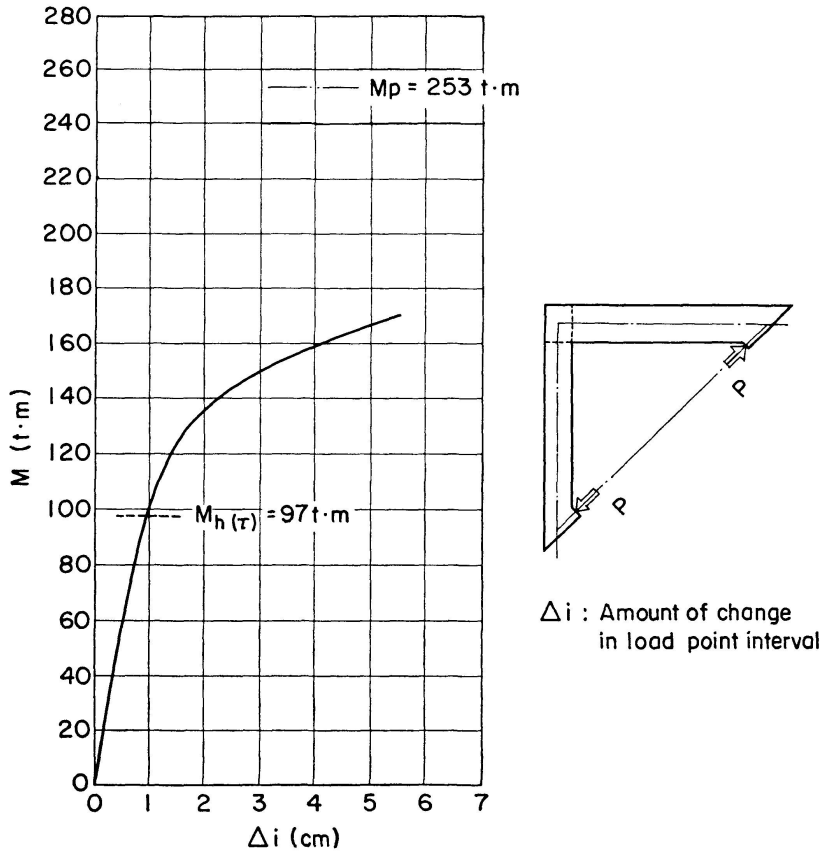

Fig. 9.

point interval. According to this diagram, the yield condition is satisfied by the bending moment $M_{h(\tau)}$ derived from $\tau_y = 0.45\,\sigma_y$ in the knee joint, giving no play to the total plastic moment M_p.

That is to say, the yield condition is satisfied by the shearing force in this type of knee joint, resulting in a possible lowering of the total plastic moment in the column or beam. Therefore, it is necessary to pay careful attention to the thickness of the web at the knee joint.

Great stress concentration is brought about in the proximity of the inner point in the knee joint. This makes it necessary to keep the welded joining part transmissible of the total strength of the plate.

As the stress concentration due to shear lag is reduced by increasing the web at the knee joint in thickness, any consideration given to shearing force in the knee joint will also have an effect on the stress concentration in the proximity of the inner point.

1.4. Application to Other Types

A straight haunch type knee joint is seen when an increase in the height of a web is limited to the proximity of the knee joint to cope with great bending moment exerted on it. It is also applied to the middle column in a multi-span rigid frame to which beams are joined at somewhat different heights from each other (Fig. 10).

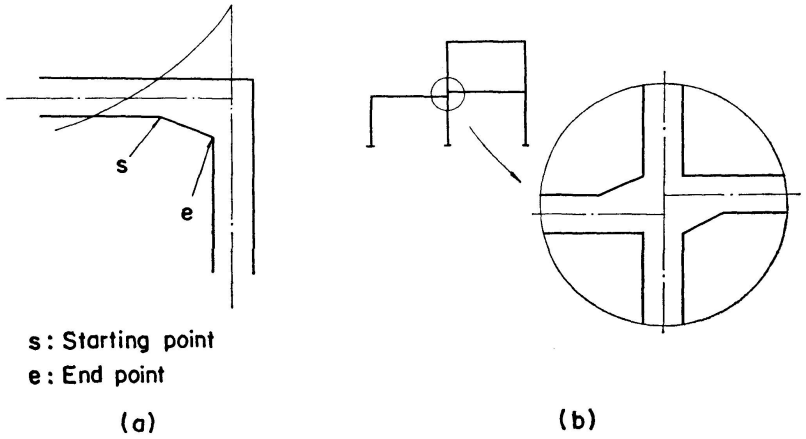

Fig. 10.

In this type, stress concentration at the starting or end point of the straight haunch comes into question. The stress at this point is presumed to be affected considerably by the haunch angle, the radius of curvature R of a flange and the use of a diaphragm at the starting point or end point of the haunch.

It is of great importance for designers to give a detailed experimental examination to these factors. So far as the present author knows, the results of experiments on the straight haunch type knee joint in members of box section have not been published.

Shearing stress in webs of this type is treated in the same way as that in straight rectangular type knee joints.

F_{01}, F_{i1}, F_{02} and F_{i2} are the same as given in Eq. (1). From Fig. 11

$$Q_2 = N_1, \qquad Q_1 = N_2 - F_{i1}\tan\theta. \tag{28}$$

From Eq. (28)

$$\tau_{01} = \frac{F_{01}}{2d_2t_2}, \qquad \tau_{i1} = \frac{F_{i1}-Q_2}{2d_2t_2} = \tau_{01},$$
$$\tau_{02} = \frac{F_{02}}{2d_1't_2}, \qquad \tau_{i2} = \frac{F_{i2}-F_{i1}\tan\theta-Q_1}{2d_1't_2} = \tau_{02}. \tag{29}$$

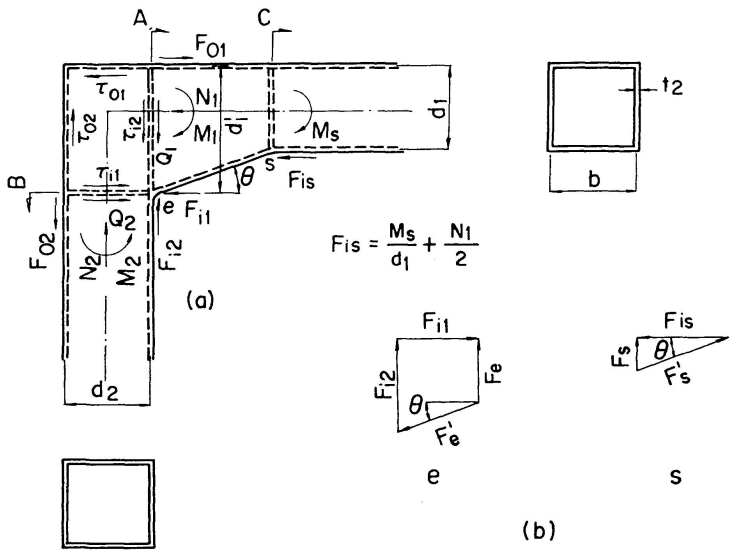

Fig. 11.

The axial stress in flanges of this type can be calculated in the same way as that in the above-mentioned straight rectangular type.

Suppose that the forces acting on the points e and s in Fig. 11 (a) are arranged as shown in Fig. 11 (b) and the resultant forces are concentrated in the sections A and C. According to this figure,

$$F_e = F_{i2} - F_{i1} \tan\theta, \qquad F_S = F_{iS} \tan\theta. \tag{30}$$

Stress due to shear lag in the sections A, B and C are defined respectively as

$$\sigma_{S1} = \frac{b}{d_1'} \frac{F_e}{A_{w1}} S_1, \qquad \sigma_{S2} = \frac{b}{d_2} \frac{F_{i1}}{A_{w2}} S_2, \qquad \sigma_{SC} = \frac{b}{d_1} \frac{F_S}{A_{wC}} S_C, \tag{31}$$

where S_1, S_2 and S_C can be found from the above-mentioned estimated dia-

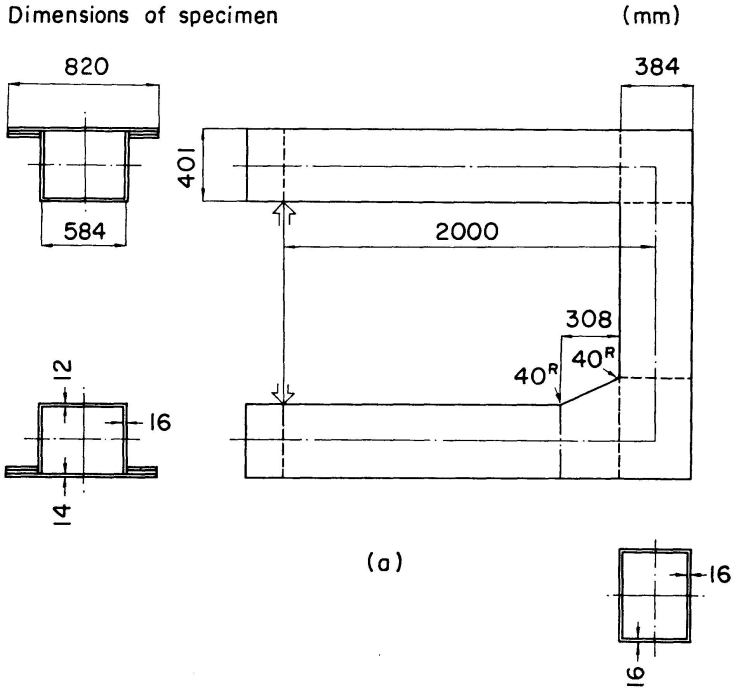

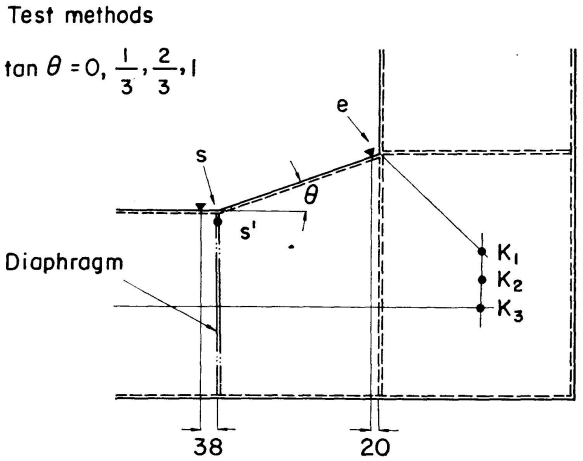

▼ : Axial stress in the flange
● : Shearing stress in the web

Fig. 12.

grams used for estimating the stress due to shear lag with respect to R_S of the respective sections.

In this case, the section C in which the starting point of the haunch lies is provided with a diaphragm.

The results of experiments in this type are illustrated in Fig. 12, 13 and 14.

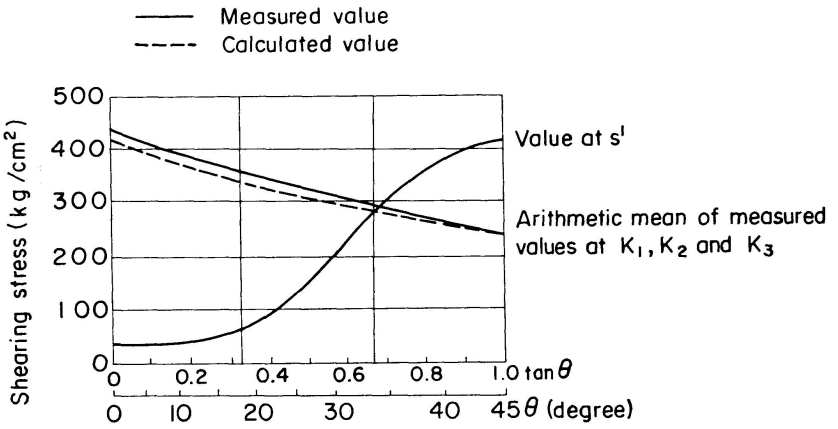

Fig. 13.

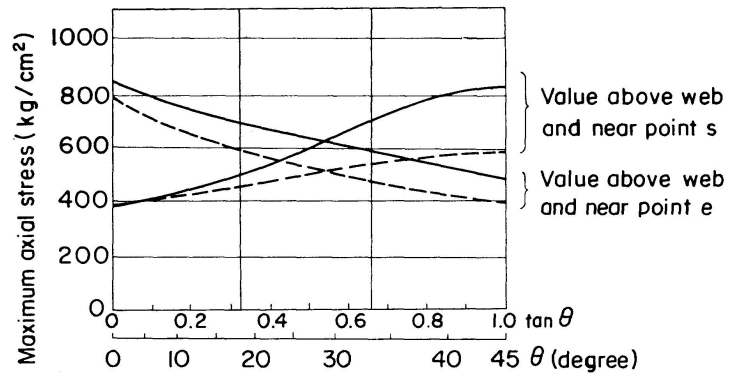

Fig. 14.

According to these figures, shearing stress in the knee joint decreases and shearing stress in the part in which the starting point of the haunch lies increases with an increase in haunch angle. The calculated values of shearing stress in the knee joint come nearly in coincidence with the measured values. With an increase in haunch angle, the maximum axial stress in the flanges increases in the section in which the starting point of the haunch lies but decreases in the section in which the end point of the haunch lies. The calculated values of the maximum axial stress in the flanges are a little smaller than the measured values, while they show practically the same tendency with regard to variation with a change in haunch angle. As the specimens used in this experiment are devised to show a difference caused by the presence of a diaphragm in the section C, the diaphragm is designed to be removably attached to the section C with bolts. Judging from the fact that sizable deformation was found in the section C even when a diaphragm was attached to the section in this experiment, the large measured values in the section where the starting point

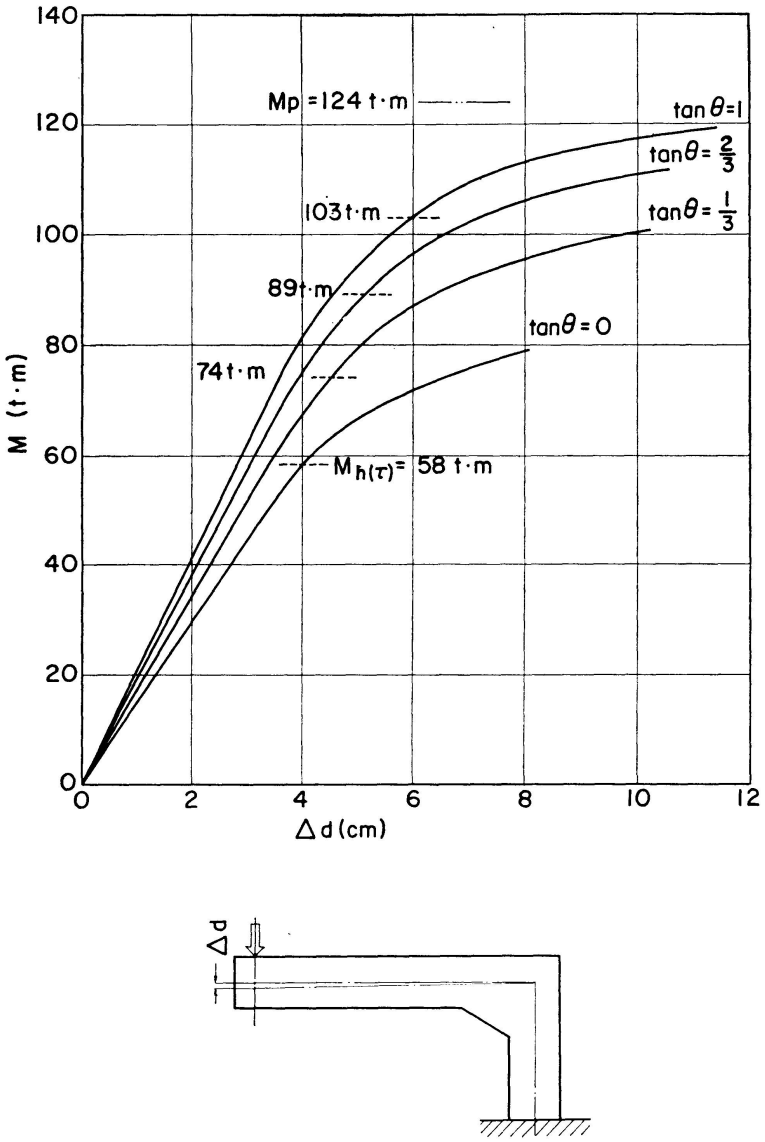

Fig. 15.

of the haunch with large haunch angel lies may be attributed mainly to how fightly the diaphragm is bolted.

An $M-\Delta d$ curve is shown in Fig. 15. According to this figure, these initial yields arise, for the most part, at $M_{h(\tau)}$, indicating that careful attention must be paid to the thickness of webs at this point in a knee joint as in the case of the straight rectangular type. A fairly large value of $M_{h(\tau)}$ can be expected by enlarging the haunch angle. The local shearing stress at the starting point of the haunch has a less effect on $M_{h(\tau)}$ and Δd than the shearing stress in the whole knee joint.

The application of this theory to straight flanges at an arc knee joint will be described hereinafter. (The calculation of stress in circular arc flanges at circular arc knee joints will be described in Chapter 3.)

Assuming that flange force is uniformly distributed in the arc part, the

distributed load F_i/R_i acts in the normal direction of the flange as shown in Fig. 16 (b). Let the rigid frame be substituted by a beam, and the force down $F_i \Delta\theta \sin\theta$ will act on Δx as shown in Fig. 16 (a), placing the beam under the distributed load $\frac{F_i \Delta\theta \sin\theta}{\Delta x} = \frac{F_i}{R_i}$ within $d \leqq x \leqq d + R_i$.

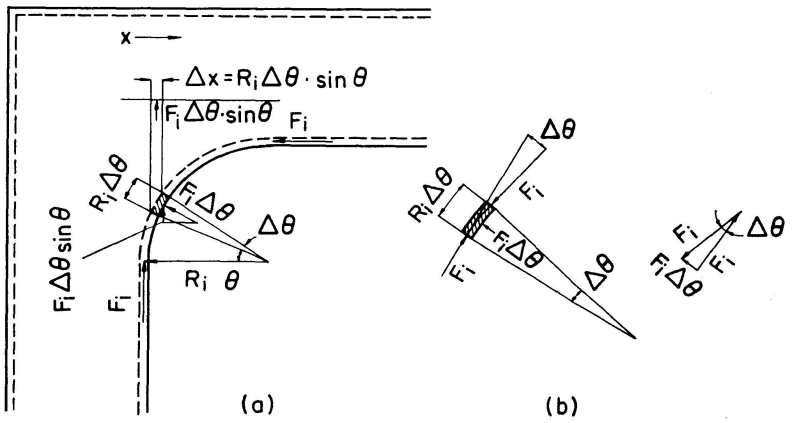

Fig. 16.

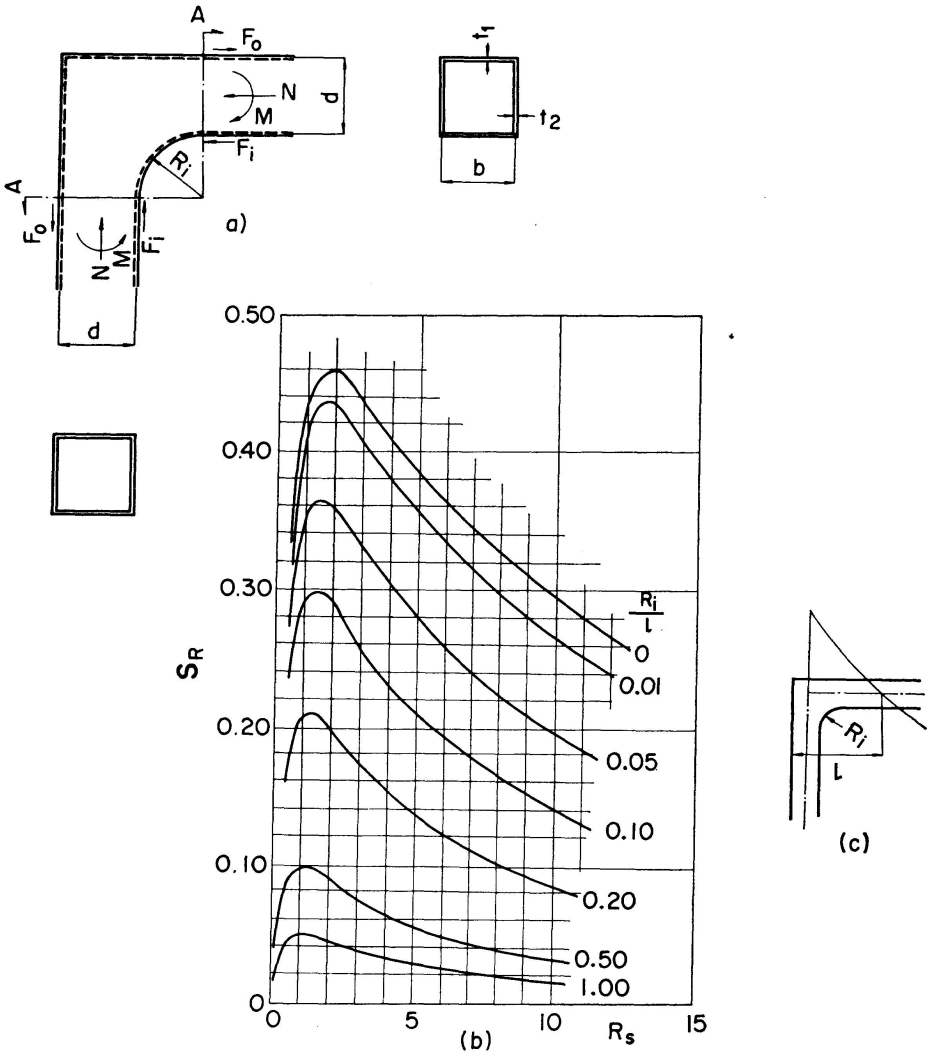

Fig. 17.

Expanding the moment acting on the beam into Fourier series

$$M = \frac{4l^2}{\pi^3}\frac{F_i}{R_i}\sum_{n=1}^{\infty}\frac{1}{n^3}\sin\left\{\zeta_n\left(d+\frac{R_i}{2}\right)\right\}\sin\frac{\zeta_n R_i}{2}\sin(\zeta_n x), \tag{32}$$

where

$$\zeta_n = \frac{n\pi}{l}. \tag{33}$$

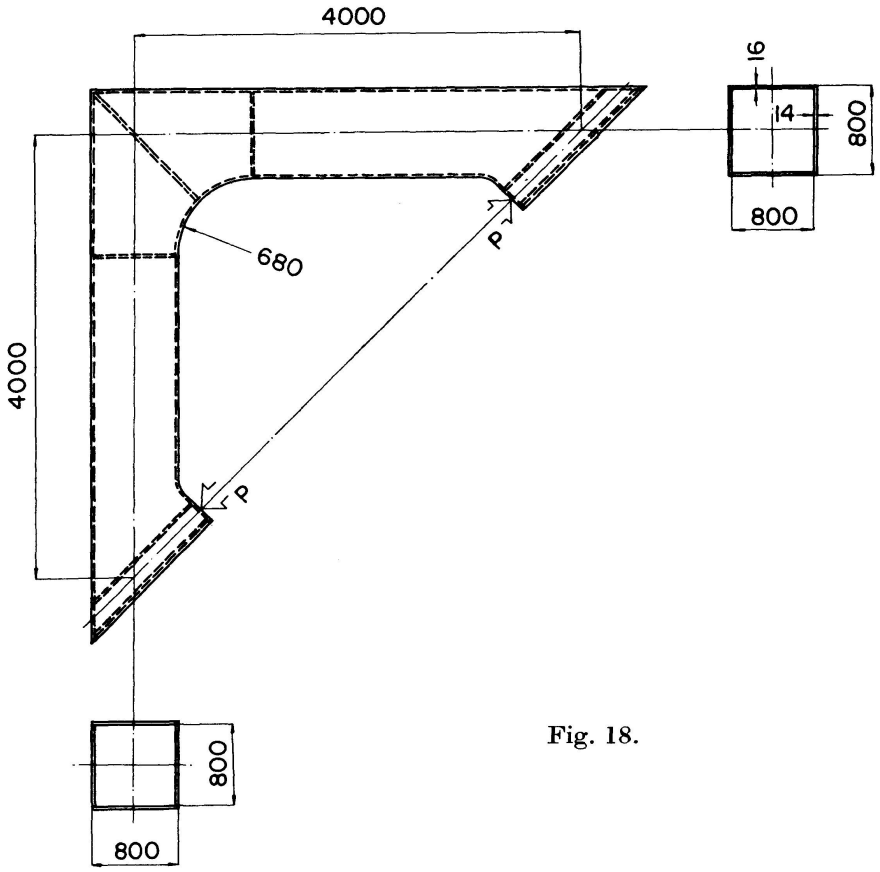

Fig. 18.

Let us find out the stress due to shear lag according to the method described in Section 1—2. When the distributed load F_i/R_i is applied in the middle of the span of a simple beam over the length of R_i, the bending moment in the middle of the span can be written in the form

$$M = \frac{2F_i l}{\pi^2}\sum_{n=1}^{\infty}\frac{1}{n^2}\frac{\sin\frac{n\pi R_i}{2l}}{\frac{n\pi R_i}{2l}}, \quad (n = 1, 3, 5, \ldots), \tag{34}$$

$$\left(\frac{1}{S_n}-\frac{1}{S}\right) = \frac{3}{A_w d'}\frac{R_S}{1+R_S}\frac{1-\frac{b'_n}{b'}}{1+\frac{b'_n}{b'}R_S},$$

$$\sigma_S = M\left(\frac{1}{S_n}-\frac{1}{S}\right) = \frac{F_i b'}{A_w d'}\sum_{n=1}^{\infty}\frac{6}{\pi^2}\frac{l}{b'}\frac{R_S}{1+R_S}\frac{1-\frac{b'_n}{b'}}{1+\frac{b'_n}{b'}R_S}\frac{1}{n^2}\frac{\sin\frac{n\pi R_i}{2l}}{\frac{n\pi R_i}{2l}} = \frac{b}{d}\frac{F_i}{A_w}S_R, \tag{35}$$

where $$S_R = \sum_{n=1}^{\infty} \frac{6}{\pi^2} \frac{l}{b'} \frac{R_S}{1+R_S} \frac{1-\frac{b'_n}{b'}}{1+\frac{b'_n}{b'}R_S} \frac{1}{n^2} \frac{\sin\frac{n\pi R_i}{2l}}{\frac{n\pi R_i}{2l}}, \quad (n = 1, 3, 5, \ldots). \quad (36)$$

Therefore, the estimated diagram shown in Fig. 17 (b) can be obtained for shear lag in the straight flange at the arc knee joint. In this diagram, the curve for $R_i/l = 0$ is identical with the one shown in Fig. 4. The result of measurement of the straight flange of this type used in the experiment is shown in Fig. 19. The calculated values are fairly close to the measured values.

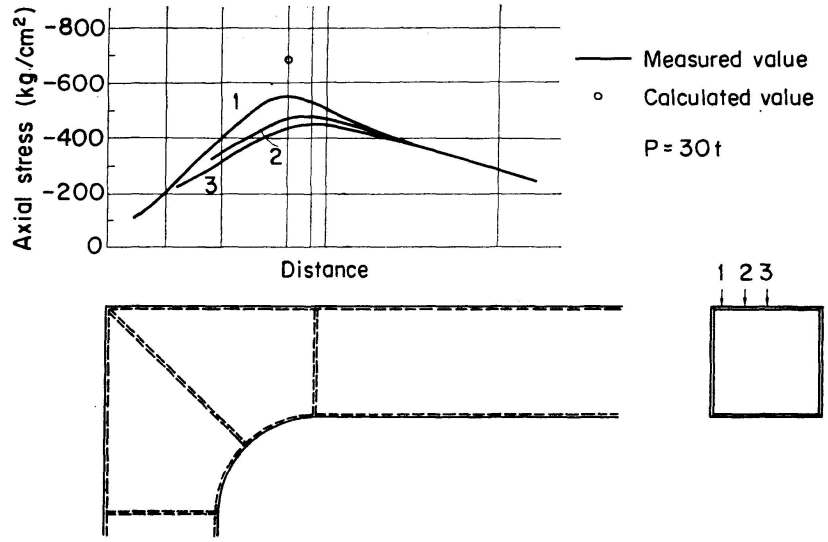

Fig. 19.

2. Knee Joint in Which a Cylinder is Used as a Column

The type in which a cylinder is used as a column has been adopted in various places. The use of a cylinder as a column is attributed to its fine appearance, its excellence in local buckling and torsional resistance featuring the cylindrical construction and its section characteristics free from directionality.

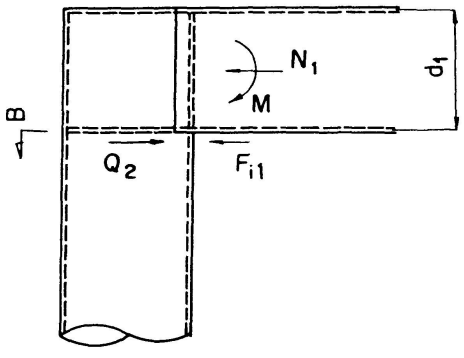

Fig. 20.

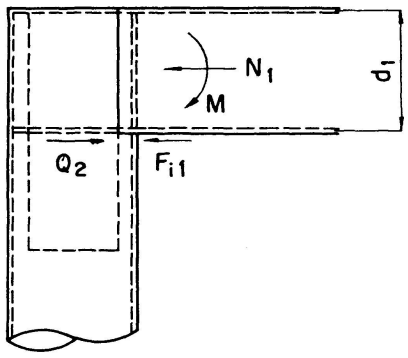

Fig. 21.

This type of knee joint has two varieties, one having the beam web butted to the cylinder and the other having the beam web interlocked with the cylinder (Fig. 20 and 21). Although the one having the beam web interlocked with the cylinder is complicated and hard to manufacture, the cylinder at the knee joint can be reduced in thickness to some extent because the thickness of the interlocked web can be taken into consideration in calculating shearing stress at the knee joint.

Shear lag must be taken into consideration in calculating the bending stress of the beam as in the case of the straight type, while the circumferential stress at the point on which beam flange force acts and the stress of a diaphragm must be taken into account in calculating the stress of the column.

Shearing Stress of Cylinder

The case in which the web of a beam is simply butted to the side of a cylindrical column:

Shearing stress at the knee joint can be written by referring to Fig. 22 in the form

$$\tau_1 = \frac{F_{i1}-Q_2}{\pi R t_p}\sqrt{1-\left(\frac{y}{R}\right)^2}, \qquad \tau_{1max} = \frac{F_{i1}-Q_2}{A_C} \leqq \tau_a, \tag{37}$$

$$\tau_a = 0.5\,\sigma_a, \tag{38}$$

where

$$F_{i1} = \frac{M}{d_1} + \frac{N_1}{2},$$

τ_1 = shearing stress,
τ_a = allowable shearing unit stress,
A_C = sectional area of cylinder.

A diaphragm is provided on the section of the column to which the beam flange is butted.

The case in which the web of a beam is interlocked with a cylinder:

When an opening is provided in the position shown in Fig. 23, the statically determinate shear flow function κ_0 is defined as

$$\begin{aligned} \kappa_0 &= R^2 t_p \sin\varphi, && (\varphi = 0 \sim \alpha), \\ \kappa_0 &= R^2 t_p \sin\varphi + \tfrac{1}{8} d_2^2 t_2, && (\varphi = \alpha \sim (\pi-\alpha)), \\ \kappa_0 &= R^2 t_p \sin\varphi, && (\varphi = (\pi-\alpha) \sim \pi) \end{aligned} \tag{39}$$

in the cylinder, and

$$\kappa_0 = \frac{1}{2} y^2 t_2, \qquad \left(y = 0 \sim \frac{d_2}{2}\right) \tag{40}$$

in the interlocked web.

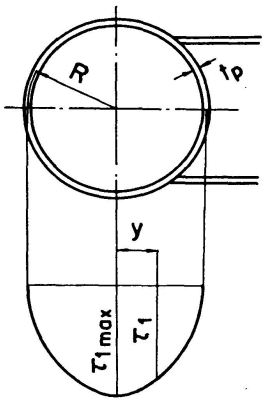

Fig. 22.

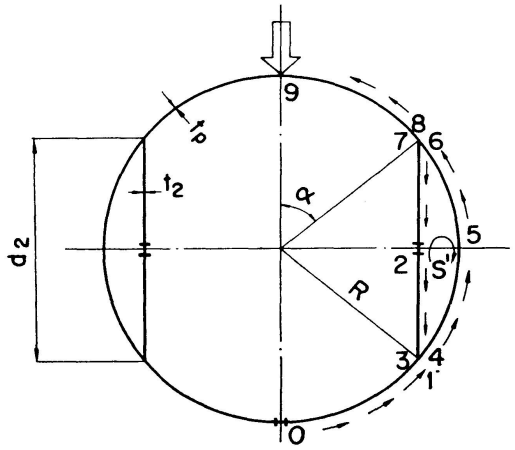

Fig. 23.

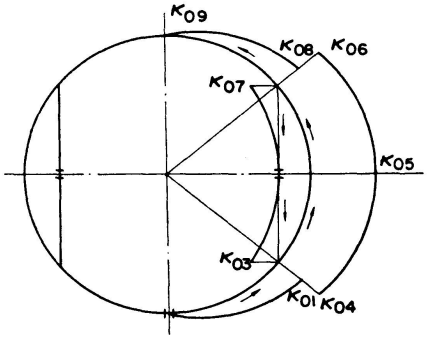

Fig. 24.

The statically indeterminate shear flow function S' attributable to closed section is defined as

$$S' \oint \frac{du}{t} + \oint \frac{\kappa_0 \, du}{t} = 0, \tag{41}$$

$$\begin{aligned} \oint \frac{\kappa_0 \, du}{t} &= \frac{1}{t_p} \int_{\alpha}^{\pi-\alpha} \left(R^2 t_p \sin\varphi + \frac{1}{8} d_2^2 t_2 \right) R \, d\varphi + \frac{2}{t_2} \int_0^{\frac{d_2}{2}} \frac{y^2}{2} t_2 \, dy \\ &= 2 R^3 \cos\alpha + \frac{t_2}{8 t_p} d_2^2 R (\pi - 2\alpha) + \frac{d_2^3}{24}, \end{aligned} \tag{42}$$

$$\oint \frac{du}{t} = \frac{R}{t_p} (\pi - 2\alpha) + \frac{d_2}{t_2}. \tag{43}$$

From Eqs. (41), (42) and (43)

$$S' = - R^2 t_2 \cos\alpha \, \frac{(2 + \frac{1}{3}\cos^2\alpha) t_p + \frac{1}{2}(\pi - 2\alpha) t_2 \cos\alpha}{(\pi - 2\alpha) t_2 + 2 t_p \cos\alpha} \tag{44}$$

at $\varphi = \alpha \sim (\pi - \alpha)$.

The shear flow function is given in the form

$$\kappa = \kappa_0 + S'. \tag{45}$$

The shearing stress in the knee joint can be written by referring to Fig. 25 in the form

$$\tau_1 = \frac{F_{i1}-Q_2}{I_x t_p}\kappa, \qquad \tau_2 = \frac{F_{i1}-Q_2}{I_x t_2}\kappa, \tag{46}$$

where I_x: geometrical moment of inertia with respect to the x-axis of the cylinder having the interlocked web,

τ_1: shearing stress of the cylinder,

τ_2: shearing stress of the interlocked web.

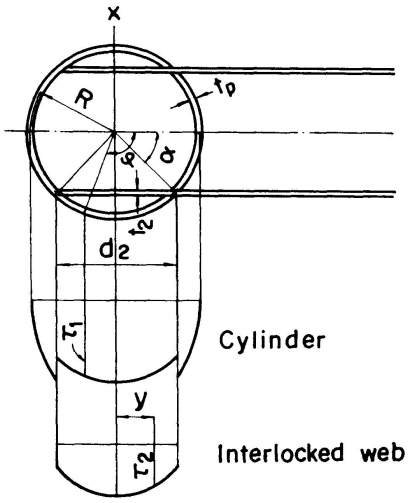

Fig. 25.

The shearing stress of the cylinder reaches its maximum value at $\varphi=\alpha$ or $\varphi=\pi/2$ as written in the form

$$\begin{aligned} \tau_{max} &= \frac{F_{i1}-Q_2}{I_x} R^2 \sin\alpha, && (\varphi=\alpha), \\ \tau_{max} &= \frac{F_{i1}-Q_2}{I_x t_p}\left(R^2 t_p + \frac{1}{8} d_2^2 t_2 + S'\right), && \left(\varphi=\frac{\pi}{2}\right). \end{aligned} \tag{47}$$

The shearing stress of the interlocking web reaches its maximum value at $\varphi=\pi/2$ as written in the form

$$\tau_{max} = \frac{F_{i1}-Q_2}{I_x t_2} S'. \tag{48}$$

Allowable shearing unit stress has been determined in accordance with the theory of the maximum shearing stress. As the maximum value obtained by measurement is practically the same as that obtained by calculation according to the result of an experiment made with this type as described later, this type differs from the straight rectangular type knee joints in that there is no necessity for estimating the allowable shearing unit stress still lower.

Flange Stress of Beam

The stress of beam flanges is calculated in the same way as described above by supposing a knee joint consisting of a column of box section in which

interlocking depth is regarded as the height of the web and the sum of the thickness of an interlocked web and that of a cylinder is regarded as the thickness of the web. The stress of beam flanges in the type in which the beam is not interlocked with the column can be calculated in the same way as mentioned above.

$$\sigma_{01} = \frac{M_1}{S_b} - \frac{N_1}{A_b}, \qquad \sigma_{i1} = \frac{M_1}{S_b} + \frac{N_1}{A_b}, \qquad \sigma_{S1} = \frac{b}{d_1}\frac{F_{i2}}{A_{w1}} S_{S1},$$

$$\sigma_{m01} = \sigma_{01} + \sigma_{S1}, \qquad \sigma_{mi1} = \sigma_{i1} + \sigma_{S1}.$$

Since the value of F_{i2} increases rapidly with an increase in the value of α by this method of calculation, it may be suggested to substitute the distance between centroids in the circular arc for the interlocking depth as d_2 as shown in Fig. 26 (b).

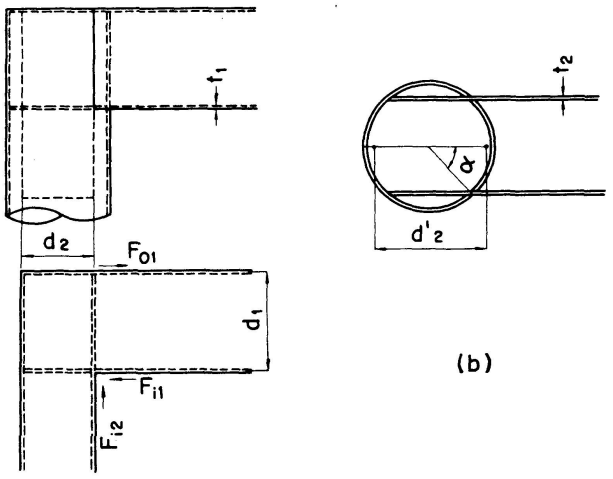

Fig. 26.

However, in the case of $\alpha = 50°$, the value of the maximum stress of the flanges calculated by d_2 is closer to the measured value than that calculated by d_2', the value calculated by d_2' being smaller than the measured value. The practical value of α is found to range from 45° to 55° according to the sectional dimensions of beams and the detailed design of joints. Within this range, the value of F_{i2} will not increase rapidly.

Circumferential Stress of the Cylinder and the Stress of the Diaphragm

The cylindrical column of this type must be examined carefully.

When diaphragms are provided on the section of a cylinder to which beam flanges are butted, it has been confirmed that the measured value of the axial stress of the cylindrical column is close to the calculated value based on the conventional beam theory. It is proposed to prove circumferential stress in the following way in providing the section of a cylinder with diaphragms.

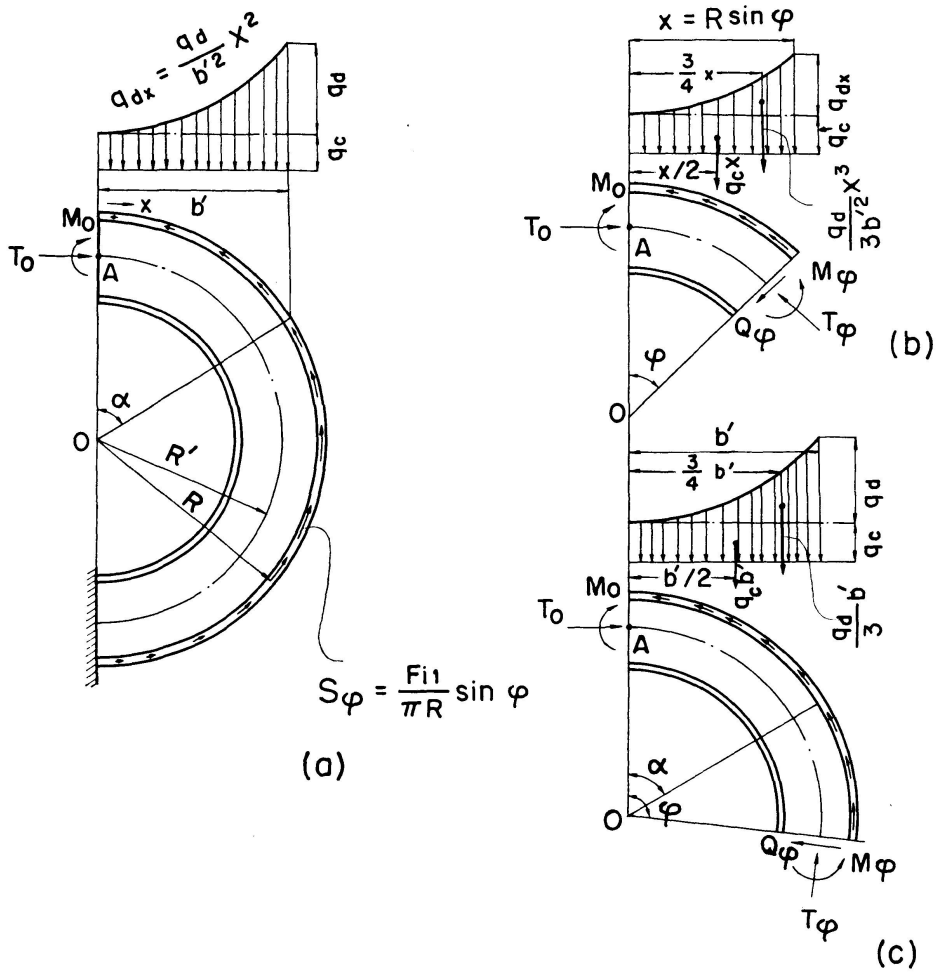

Fig. 27.

The load which is put on a cylindrical column is assumed to be distributed in the form of quadratic parabola over the width of beam flanges as shown in Fig. 27.

$$q = q_C + \frac{q_d}{b'^2} x^2. \tag{49}$$

The resultant force F_{i1} of the load can be written in the form

$$F_{i1} = 2 \int_0^{b'} q \, dx = 2b' \left(q_C + \frac{q_d}{3} \right). \tag{50}$$

It is assumed that F_{i1} is balanced by the shear flow S_φ in the section of the cylinder.

$$S_\varphi = \frac{F_{i1}}{\pi R} \sin\varphi, \tag{51}$$

where R is the radius of the cylinder extending to the center line of the thickness of its wall.

Let T_0 and M_0 be statically indeterminate axial force and bending moment as shown in Fig. 27. We obtain,

when $0 \leqq \varphi \leqq \alpha$

$$T_\varphi = T_0 \cos\varphi - \frac{F_{i1}}{2\pi}\varphi \sin\varphi + q_C R \sin^2\varphi + \frac{q_d}{3b'^2} R^3 \sin\varphi, \tag{52}$$

$$\begin{aligned} M_\varphi = {} & M_0 + T_0 R'(1-\cos\varphi) - \frac{F_{i1} R}{\pi}\left(1-\cos\varphi - \frac{R'}{2R}\varphi\sin\varphi\right) \\ & - R\left(R' - \frac{R}{2}\right) q_C \sin^2\varphi - \frac{q_d}{3b'^2} R^3 \left(R' - \frac{3}{4}R\right)\sin^4\varphi, \end{aligned} \tag{53}$$

$$Q_\varphi = T_0 \sin\varphi - \frac{F_{i1}}{2\pi}(\sin\varphi - \varphi\cos\varphi) - q_C R \sin\varphi\cos\varphi - \frac{q_d}{3b'^2} R^3 \sin^3\varphi\cos\varphi, \tag{54}$$

when $\alpha \leqq \varphi \leqq \pi$

$$T_\varphi = T_0 \cos\varphi - \frac{F_{i1}}{2\pi}\varphi\sin\varphi + \frac{F_{i1}}{2}\sin\varphi, \tag{55}$$

$$\begin{aligned} M_\varphi = {} & M_0 + T_0 R'(1-\cos\varphi) - \frac{F_{i1} R}{\pi}\left(1-\cos\varphi - \frac{R'}{2R}\varphi\sin\varphi\right) \\ & - q_C b'\left(R'\sin\varphi - \frac{b'}{2}\right) - \frac{q_d}{3} b'\left(R'\sin\varphi - \frac{3}{4}b'\right) \\ = {} & M_0 + T_0 R'(1-\cos\varphi) - \frac{F_{i1} R}{\pi}\left(1-\cos\varphi - \frac{R'}{2R}\sin\varphi\right) \\ & - \frac{F_{i1} R'}{2}\sin\varphi + \frac{b'^2}{4}(2q_C + q_d), \end{aligned} \tag{56}$$

$$Q_\varphi = T_0 \sin\varphi - \frac{F_{i1}}{2\pi}(\sin\varphi - \varphi\cos\varphi) - \frac{F_{i1}}{2}\cos\varphi. \tag{57}$$

Rewriting T_φ, M_φ and Q_φ in terms of $k = F_C{}^*)/F_{i1}$ and $\lambda = R/R'$,

when $0 \leqq \varphi \leqq \alpha$

$$T_\varphi = T_0 \cos\varphi - \frac{F_{i1}}{2}\left(\frac{\varphi}{\pi}\sin\varphi - \frac{k}{\sin\alpha}\sin^2\varphi - \frac{1-k}{\sin^3\alpha}\sin^4\varphi\right), \tag{58}$$

$$\begin{aligned} M_\varphi = {} & M_0 + R'\left[T_0(1-\cos\varphi) - \frac{F_{i1}}{2}\left\{\frac{2\lambda}{\pi}(1-\cos\varphi) - \frac{\varphi}{\pi}\sin\varphi\right.\right. \\ & \left.\left. + \frac{k\left(1-\frac{\lambda}{2}\right)}{\sin\alpha}\sin^2\varphi + \frac{(1-k)\left(1-\frac{3}{4}\lambda\right)}{\sin^3\alpha}\sin^4\varphi\right\}\right], \end{aligned} \tag{59}$$

$$Q_\varphi = T_0 \sin\varphi - \frac{F_{i1}}{2}\left\{\frac{1}{\pi}(\sin\varphi - \varphi\cos\varphi) + \frac{k}{\sin\alpha}\sin\varphi\cos\varphi + \frac{1-k}{\sin^3\alpha}\sin^3\varphi\cos\varphi\right\}, \tag{60}$$

---

*) $F_C = 2 q_C b'$ and $k = \dfrac{q_C}{q_C + \frac{q_d}{3}} = \dfrac{\sigma_{i1} - \frac{1}{2}\sigma_{S1}}{\sigma_{i1}} = \dfrac{2\sigma_{i1} - \sigma_{S1}}{2\sigma_{i1}}$ in Fig. 27 (a) and 28 (a).

when $\alpha \leqq \varphi \leqq \pi$

$$T_\varphi = T_0 \cos\varphi - \frac{F_{i1}}{2}\left(\frac{\varphi}{\pi} - 1\right)\sin\varphi, \tag{61}$$

$$M_\varphi = M_0 + R'\left[T_0(1-\cos\varphi) - \frac{F_{i1}}{2}\left\{\frac{2\lambda}{\pi}(1-\cos\varphi) - \frac{\varphi}{\pi}\sin\varphi + \sin\varphi - \frac{\lambda(3-k)}{4}\sin\alpha\right\}\right], \tag{62}$$

$$Q_\varphi = T_0 \sin\varphi - \frac{F_{i1}}{2}\left\{\frac{1}{\pi}(\sin\varphi - \varphi\cos\varphi) + \cos\varphi\right\}. \tag{63}$$

Assuming that M_φ, T_φ and Q_φ have plus signs in the direction shown in Fig. 27 (b) and (c), the total energy V of the curved beam can be written in the form

$$V = \int_0^\pi \left(\frac{M_\varphi^2}{2EeR'} + \frac{T_\varphi^2}{2A_rE} + \frac{M_\varphi T_\varphi}{A_rER'} + \frac{Q_\varphi^2}{2A_dG}\right) R'\,d\varphi. \tag{64}$$

From Castigliano's theorem in which it is conditioned that the point A will neither rotate nor be displaced in the x-direction

$$\frac{\partial V}{\partial M_0} = 0, \tag{65}$$

$$\frac{\partial V}{\partial T_0} = 0. \tag{66}$$

From Eq. (65)

$$\frac{\partial V}{\partial M_0} = \int_0^\pi \left\{\frac{M_\varphi}{A_rEeR'}\frac{\partial M_\varphi}{\partial M_0} + \frac{T_\varphi}{A_rE}\frac{\partial T_\varphi}{\partial M_0} + \frac{M_\varphi}{A_rER'}\frac{\partial T_\varphi}{\partial M_0} + \frac{T_\varphi}{A_rER'}\frac{\partial M_\varphi}{\partial M_0} + \frac{Q_\varphi}{A_dG}\frac{\partial Q_\varphi}{\partial M_0}\right\} R'\,d\varphi = 0. \tag{67}$$

By inserting $\frac{\partial M_\varphi}{\partial M_0} = 1$, $\frac{\partial T_\varphi}{\partial M_0} = 0$ and $\frac{\partial Q_\varphi}{\partial M_0} = 0$ into Eq. (67), we obtain

$$\frac{\partial V}{\partial M_0} = \int_0^\pi \left\{\frac{M_\varphi}{A_rEeR'} + \frac{T_\varphi}{A_rER'}\right\} R'\,d\varphi = \frac{1}{A_rEe}\left\{\int_0^\pi M_\varphi\,d\varphi + e\int_0^\pi T_\varphi\,d\varphi\right\} = 0. \tag{68}$$

Hence

$$\int_0^\pi M_\varphi\,d\varphi + e\int_0^\pi T_\varphi\,d\varphi = 0. \tag{69}$$

From Eq. (69)

$$\pi M_0 = -\pi R' T_0 + F_{i1}R'\left[\lambda + \left\{\frac{1}{8}\left(1 - \frac{e}{R'}\right)(3-k) + \frac{\lambda}{24}(4-k)\right\}\cos\alpha + \frac{k}{4}\left(1 - \frac{e}{R'} - \frac{\lambda}{2}\right)\frac{\alpha}{\sin\alpha} + \frac{3(1-k)}{16}\left(1 - \frac{e}{R'} - \frac{3}{4}\lambda\right)\frac{\alpha}{\sin^3\alpha} - \frac{3(1-k)}{16}\left(1 - \frac{e}{R'} - \frac{3}{4}\lambda\right)\frac{\cos\alpha}{\sin^2\alpha} - \frac{3-k}{8}\lambda(\pi-\alpha)\sin\alpha\right]. \tag{70}$$

From Eq. (66)

$$\frac{\partial V}{\partial T_0} = \int_0^{\pi} \left\{ \frac{M_\varphi}{A_r E e R'} \frac{\partial M_\varphi}{\partial T_0} + \frac{T_\varphi}{A_r E} \frac{\partial T_\varphi}{\partial T_0} + \frac{M_\varphi}{A_r E R'} \frac{\partial T_\varphi}{\partial T_0} + \frac{T_\varphi}{A_r E R'} \frac{\partial M_\varphi}{\partial T_0} + \frac{Q_\varphi}{A_d G} \frac{\partial Q_\varphi}{\partial T_0} \right\} R' d\varphi = 0. \tag{71}$$

By inserting $\frac{\partial M_\varphi}{\partial T_0} = R'(1-\cos\varphi)$, $\frac{\partial T_\varphi}{\partial T_0} = \cos\varphi$ and $\frac{\partial Q_\varphi}{\partial T_0} = \sin\varphi$ in Eq. (71)

$$\frac{1-\frac{e}{R'}}{A_r E e} \int_0^{\pi} M_\varphi \cos\varphi \, d\varphi - \frac{1}{A_d G} \int_0^{\pi} Q_\varphi \sin\varphi \, d\varphi = 0, \tag{72}$$

When $e \ll R'$, $\frac{R'\left(1-\frac{e}{R'}\right)}{A_r E e} \gg \frac{1}{A_d G}$.

It follows that

$$\int_0^{\pi} M_\varphi \cos\varphi \, d\varphi = 0. \tag{73}$$

From the above-mentioned equations

$$T_0 = \frac{F_{i1}}{\pi}\left\{\lambda - \frac{1}{4} + \frac{1}{30}(9 - 4k - 18\lambda + 8\lambda k)\sin^2\alpha\right\}, \tag{74}$$

$$\begin{aligned} M_0 = \frac{F_{i1} R'}{\pi}\Bigg[& \frac{1}{4} - \frac{1}{30}(9 - 4k - 18\lambda + 8\lambda k)\sin^2\alpha \\ & + \left\{\frac{1}{8}\left(1-\frac{e}{R'}\right)(3-k) + \frac{\lambda}{24}(4-k)\right\}\cos\alpha + \frac{k}{4}\left(1 - \frac{e}{R'} - \frac{\lambda}{2}\right)\frac{\alpha}{\sin\alpha} \\ & + \frac{3(1-k)}{16}\left(1 - \frac{e}{R'} - \frac{3}{4}\lambda\right)\left(\frac{\alpha}{\sin^3\alpha} - \frac{\cos\alpha}{\sin^2\alpha}\right) - \frac{3-k}{8}\lambda(\pi-\alpha)\sin\alpha\Bigg]. \end{aligned} \tag{75}$$

Therefore, the circumferential stress in the section B of the cylinder (Fig. 20) and the stress of the diaphragm can be derived from

$$\sigma_0 = -\frac{T_\varphi}{A_r} - \frac{M_\varphi h_1}{A_r e j}, \tag{76}$$

$$\sigma_i = -\frac{T_\varphi}{A_r} + \frac{M_\varphi h_2}{A_r e a}, \tag{77}$$

$$\tau = \frac{Q_\varphi}{A_d}, \tag{78}$$

where σ_0 is the circumferential stress of the cylinder, σ_i is the circumferential stress of the inner flange and τ is the shearing stress of the diaphragm. Generally, σ_i reaches its maximum value in the proximity of $\varphi = \pi/2$ (compression) and $\varphi = \pi$ (tension). When the value of σ_i at $\varphi = \pi/2$ is regarded as its maximum value approximately, T_φ and M_φ can be written in the form

$$T_\varphi = \frac{F_{i1}}{4},$$
$$M_\varphi = M_0 + T_0 R' - F_{i1} R' \left\{ \frac{\lambda}{\pi} + \frac{1}{4} - \frac{\lambda}{8}(3-k)\sin\alpha \right\}. \tag{79}$$

And at $\varphi = \pi$
$$T_\varphi = -T_0,$$
$$M_\varphi = M_0 + 2T_0 R' - F_{i1} R' \left\{ \frac{2\lambda}{\pi} - \frac{\lambda}{8}(3-k)\sin\alpha \right\}. \tag{80}$$

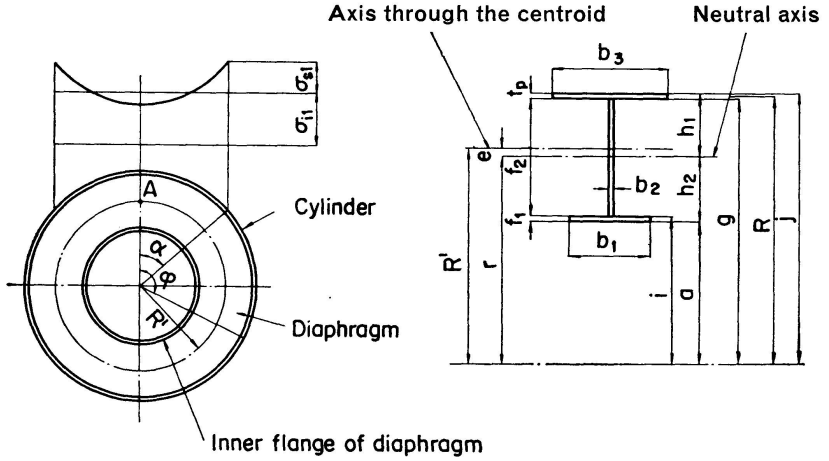

$$A_r = b_1 f_1 + b_2 f_2 + b_3 t_p, \qquad A_d = b_2 f_2, \qquad r = \frac{A_r}{b_1 \log_e \frac{i}{a} + b_2 \log_e \frac{g}{i} + b_3 \log_e \frac{j}{g}}.$$

Fig. 28.

The effective width of the cylinder shown in Fig. 28 (b) is derived from the results of experiments and the reference material [7] in the form

$$b_3 = b_2 + 1.56\sqrt{R t_p}. \tag{81}$$

The following results have been obtained according to the above-mentioned calculations:

1. Relation between α and σ_{mi1}. When the width of a beam or α is changed with the thickness of the web and the flanges of the beam and the height of the web left unchanged in the case of a cylinder with a diameter of 2 meters, σ_{mi1} of the beam flanges is calculated to reach its minimum value in the proximity of $\alpha = 45°$ and shows a large value at $\alpha \leqq 35°$ or $\alpha \geqq 60°$ (Fig. 29 (a)). Similar results are obtained in the case of a cylinder with a diameter of one meter (Fig. 29 (b)).

2. Relations between α and σ_0, σ_i and τ. When the width of a beam or α is changed with k, b_1 and b_2 left unchanged in the case of a cylinder with a diameter of 2 meters, the maximum values of σ_0, σ_i and τ are calculated to decrease with an increase in the value of α. All of them are affected greatly

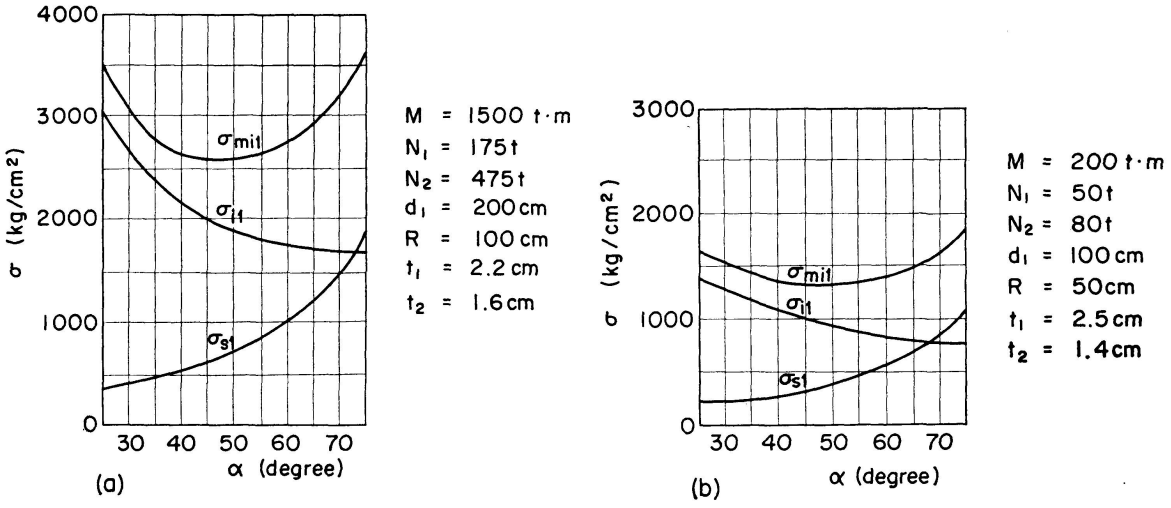

Fig. 29.

by a and decrease with a decrease in the value of a (Fig. 30 (a), (b) and (c)). The maximum value of σ_0 is more liable to be affected by t_p than the others and that of σ_i is affected by f_1 (Fig. 30 (b) and 31).

The position at which σ_i reaches its maximum value varies with α. It reaches its maximum value in the proximity of $\varphi = 76°$ for $\alpha = 45°$ and in the proximity of $\varphi = 84°$ for $\alpha = 75°$ (Fig. 30 (d)). The maximum value is affected by a for $\alpha = 45°$, but it is little affected by a for $\alpha = 75°$. Denoting σ_i at $\varphi = 90°$ by σ_{i90}, $\frac{\sigma_{imax}}{\sigma_{i90}}$ can be expressed against α as shown in Fig. 30 (e).

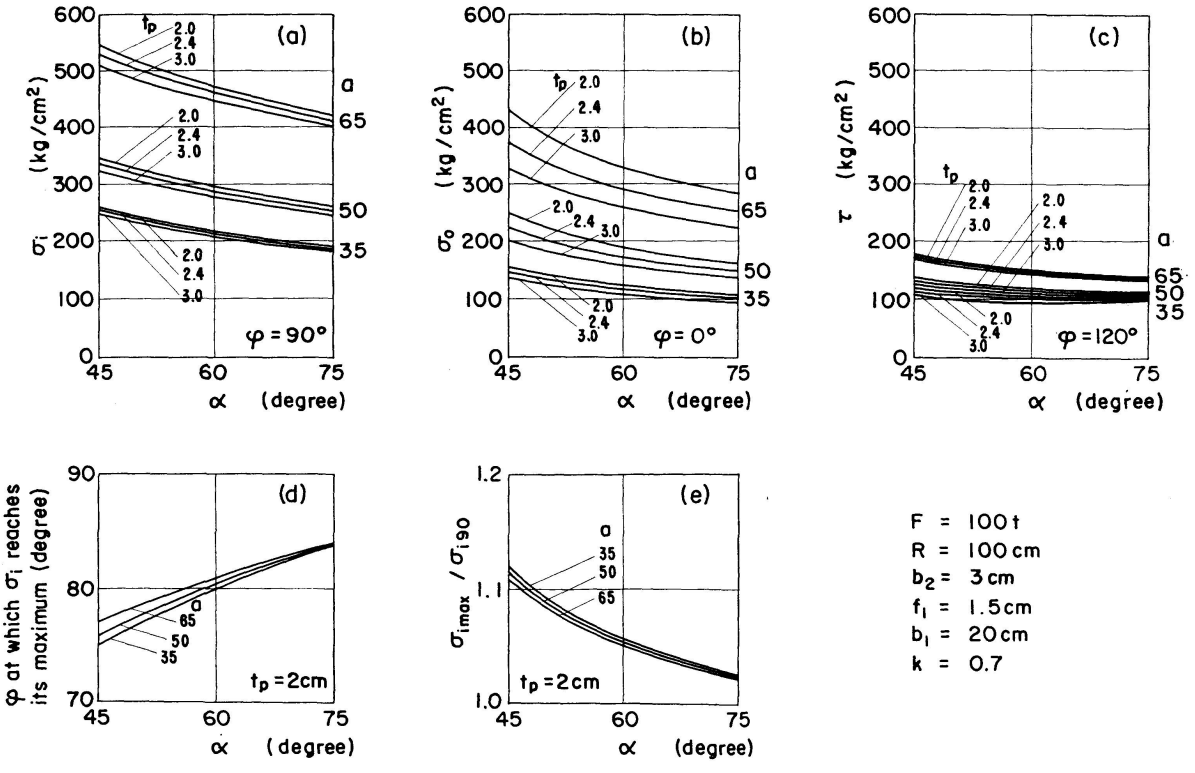

Fig. 30.

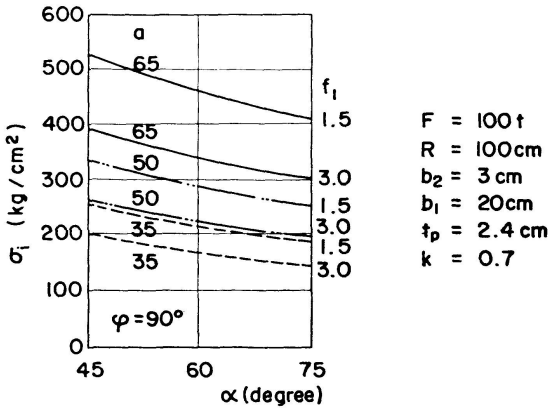

Fig. 31.

3. Relations between k and b_1 and σ_i, σ_0 and τ. σ_i increases with an increase in the value of k. However, the former is not affected greatly by the latter. Both σ_i and σ_0 decrease with an increase in the value of b_1. The effect of b_1 on σ_i is considerably great (Fig. 32).

4. Relations between $b_1 f_1$ and σ_i, σ_0 and τ. According to this method of calculation, the relations between σ_i, σ_0 and τ and $b_1 f_1$ or the area of the manhole

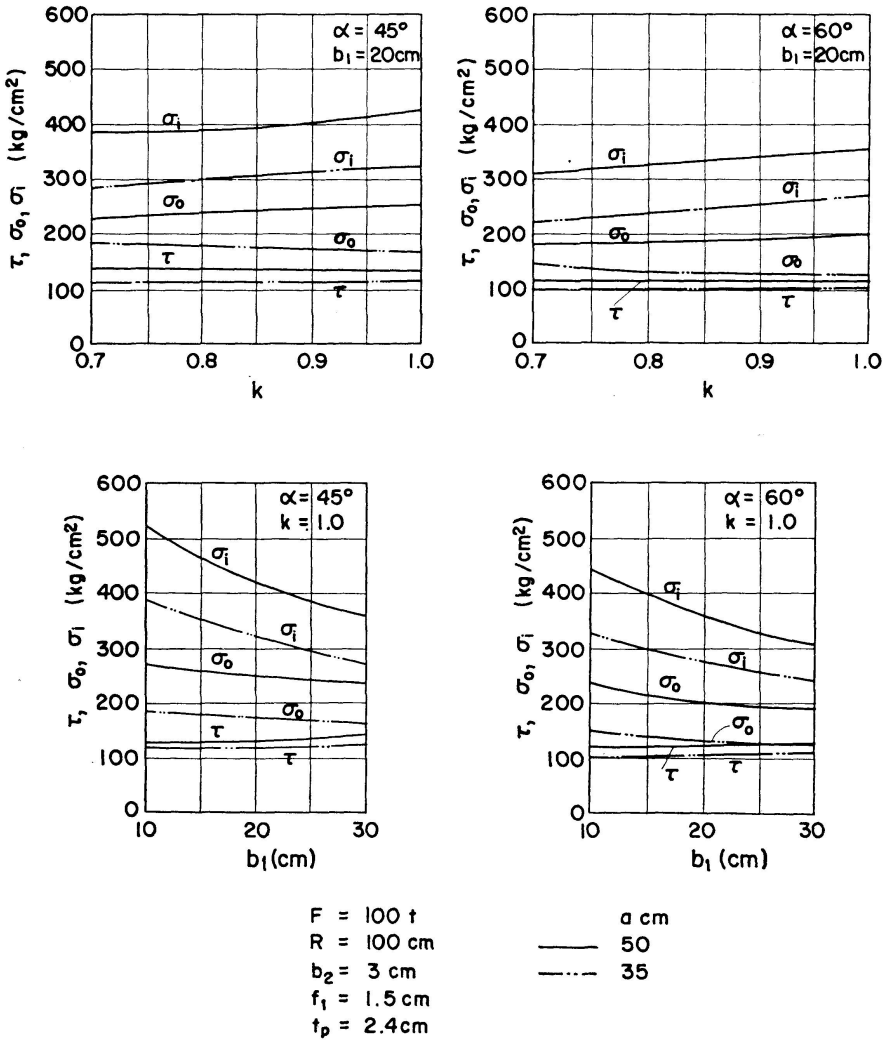

Fig. 32.

flange can be diagrammatically shown with a taken as a parameter when α, R, t_p, k and b_2 are given. An example of the relations is shown in Fig. 33. Practical values of b_1 and f_1 can be determined from such a diagram.

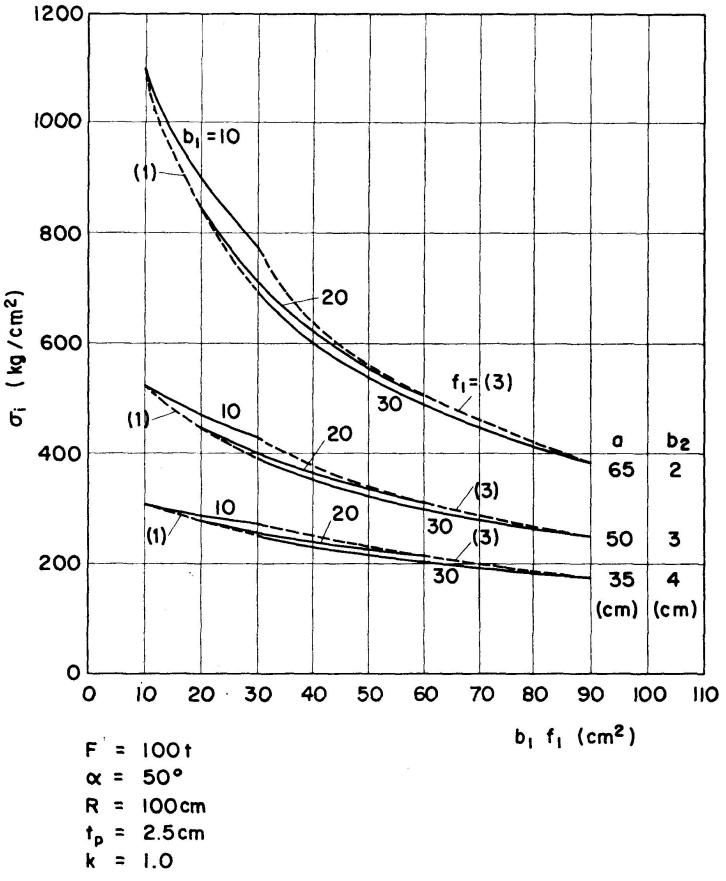

Fig. 33.

Results of Experiments

The results of experiments with this type are shown in Fig. 35 through 41. According to these results, the distribution of shearing stress is found to be disturbed in the proximity of the part at which the cylinder is joined to the beam web. The position of its maximum value lies toward the web side. The maximum value obtained by calculation is fairly close to the maximum value obtained by measurement.

The axial stress of the beam flanges is concentrated in the proximity of the web and the maximum value lies at the points where the cylinder is joined to the flanges in the axial distribution of the stress. The maximum value obtained by calculation is appropriate.

The maximum value of circumferential stress lies at the point C and that in the case of B with no interlocked webs is a little larger than that in the case of A with interlocked webs. The maximum value obtained by calculation is appropriate in the case of B.

The maximum value of the axial stress of the cylinder lies at the point D where the lower flange of the beam is joined to the cylinder. The value cal-

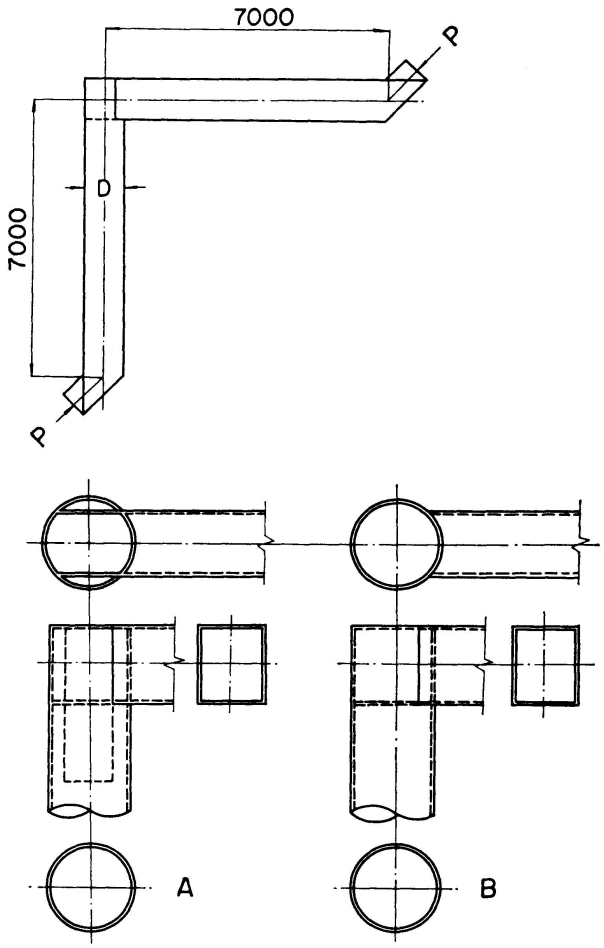

Fig. 34. With interlocked webs A
With no interlocked webs B

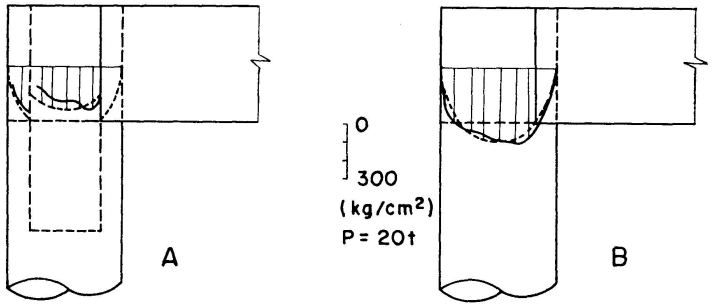

Shearing stress
—— Measured value
----- Calculated value

Fig. 35.

culated by the conventional beam theory comes in coincidence with the value measured in the proximity of the point *D*. Local bending occurs in this proximity, causing values measured on the inside and outside of the cylinder wall to differ from each other. The mean of two different values is shown in Fig. 40.

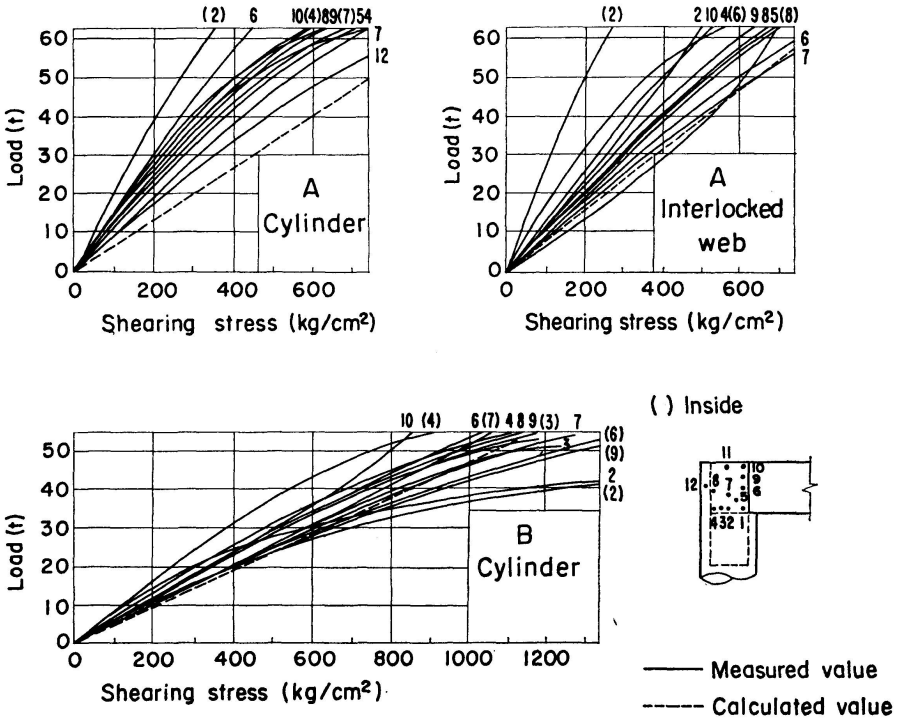

Fig. 36.

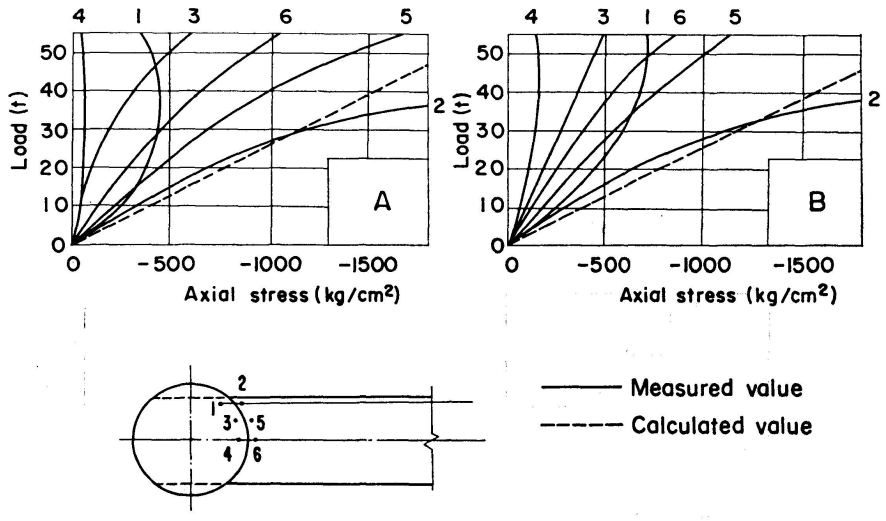

Fig. 37.

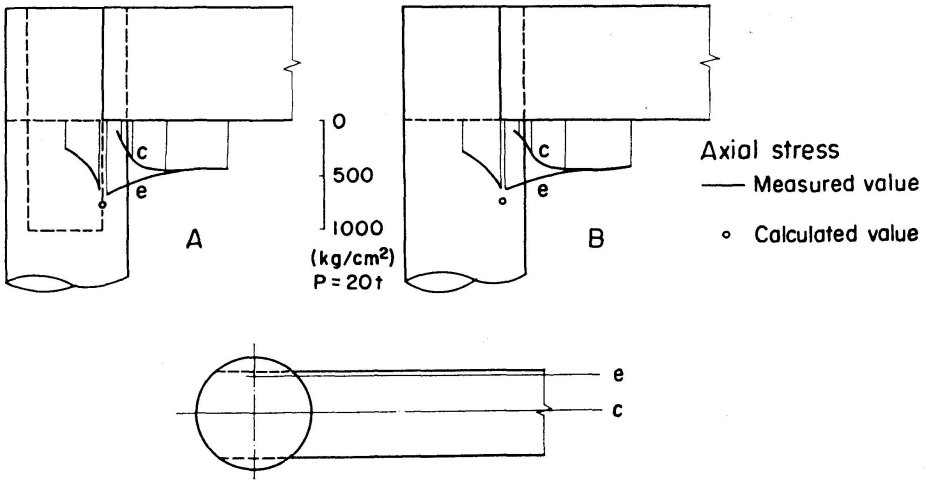

Fig. 38.

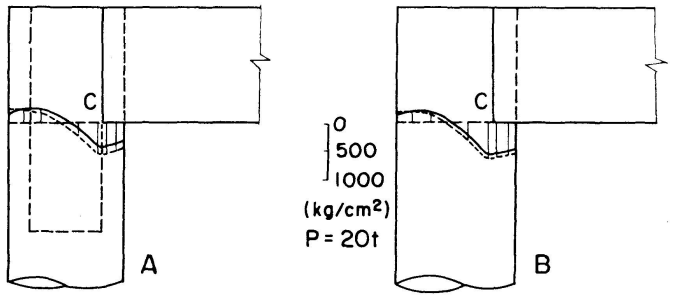

Circumferential stress

—— Measured value

----- Calculated value

Fig. 39.

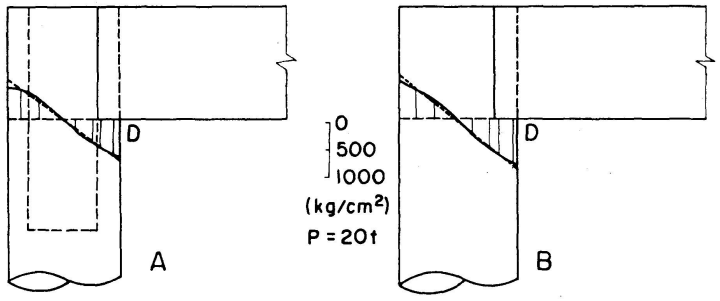

Axial stress

—— Measured value

----- Calculated value

Fig. 40.

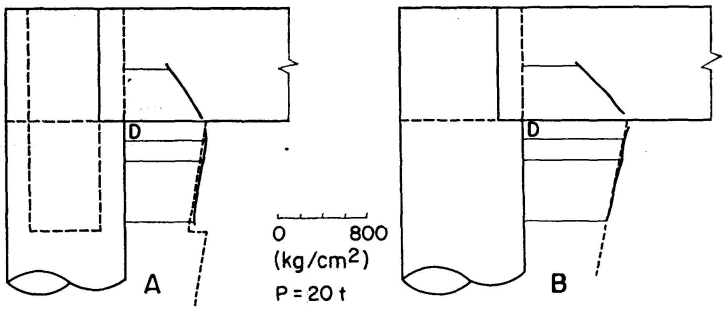

Axial stress

—— Measured value

------ Calculated value

Fig. 41.

The dimensions of the diaphragms used with the specimens are shown in Table 1.

An $M-\Delta i$ curve is given in Fig. 42. According to this curve, butting type showed initial yield in the proximity of $M_{h(\tau)}$. The interlocked web has the effect of lowering the shearing stress of the knee joint and raising the value of $M_{h(\tau)}$.

Table 1. Dimensions of the Specimen

Symbol of specimen		A	B
Outside diameter of cylinder	D (cm)	100 (radius to the center of the thickness of the cylinder wall: 49.3)	
Thickness of cylinder	t_p (cm)	1.4	
t_p/R		1/35.7	
Distance between beam flanges	d_1 (cm)	98.1	
Thickness of interlocked web	t_2 (cm)	1.4	—
Distance between beam webs	b (cm)	78.6 (total width: 85.0)	
$b/2R$		0.797	
Thickness of beam flanges	t_1 (cm)	1.9	
t_1/b		1/41.4	
Thickness of diaphragms	b_2 (cm)	1.4	
Radius of manhole a (dimensions of flange f_1, b_1) (cm)		50 (1.2,10)	
Sectional area of beam	A_b (cm²)	592.4	
Sectional area of column	A_c (cm²)	601.5	433.5
A_b/A_c		1/1.015	1/0.732
Modulus of section of beam	S_b (cm³)	19697	
Modulus of section of column	S_c (cm³)	12217	10537
S_b/S_c		1/0.620	1/0.535

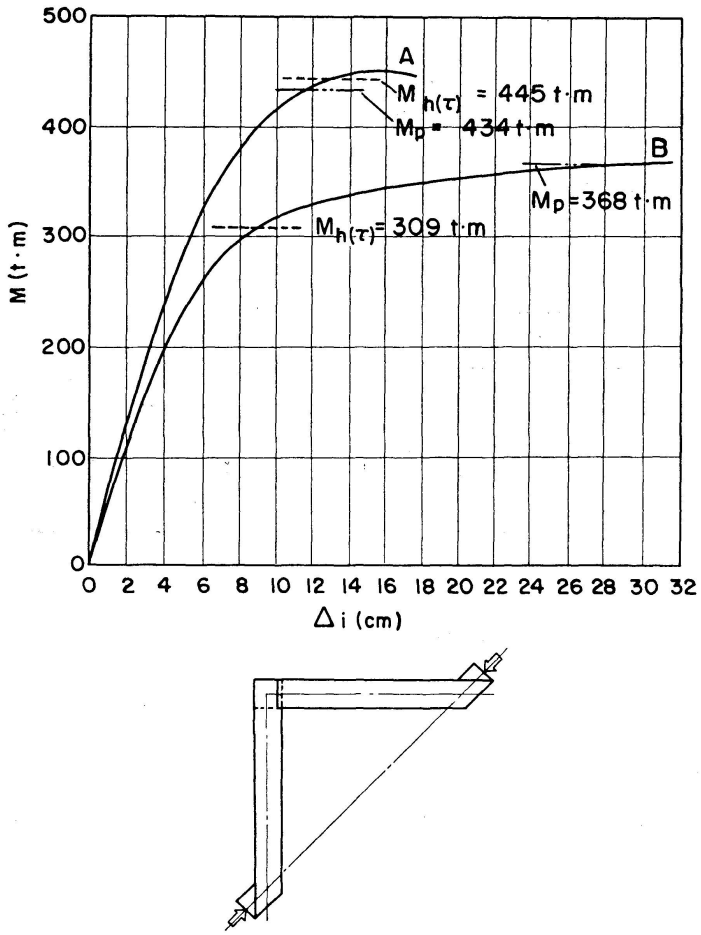

Fig. 42.

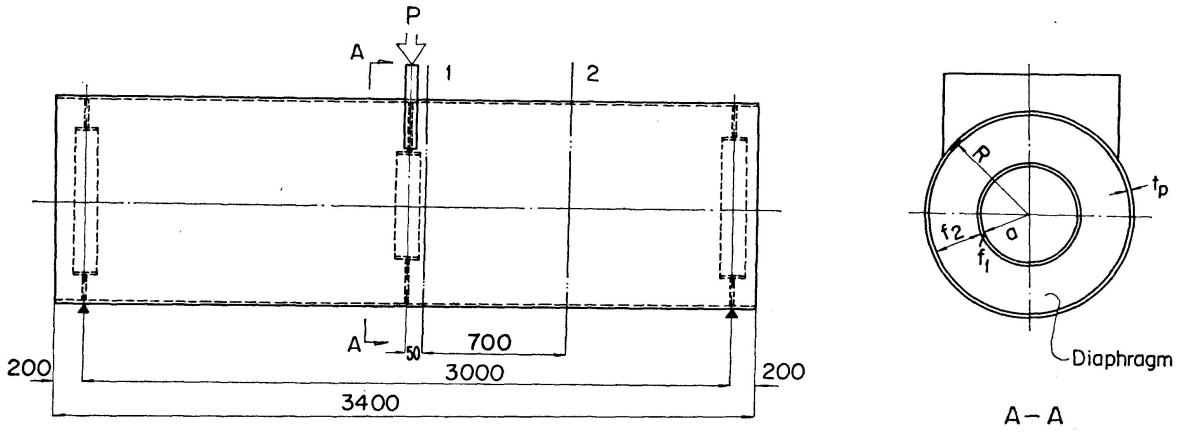

Fig. 43.

Table 2. Dimensions of the Bending Specimen

Symbol of specimen			10–350	14–350	14–500	17–350
	Outside diameter of cylinder	D (cm)	100			
	Thickness of cylinder	t_p (cm)	1.0	1.4		1.7
	t_p/R		1/49.5	1/35.2		1/28.9
	Length of span	l (cm)	300			
	Sectional area	A (cm²)	308.8	433.5		525.0
	Modulus of section	S (cm³)	7513	10537		12686
Diaphragm	Thickness of Web	b_2 (cm)	1.4			
	Radius of Manhole	a (cm)	17.5	17.5	25.0	17.5
	Dimensions of flange	f_1, b_1 (cm)	1.2,10			
	a/R		1/2.83	1/2.82	1/1.97	1/2.81
	b_2/f_2		1/21.6	1/21.3	1/16.0	1/21.1

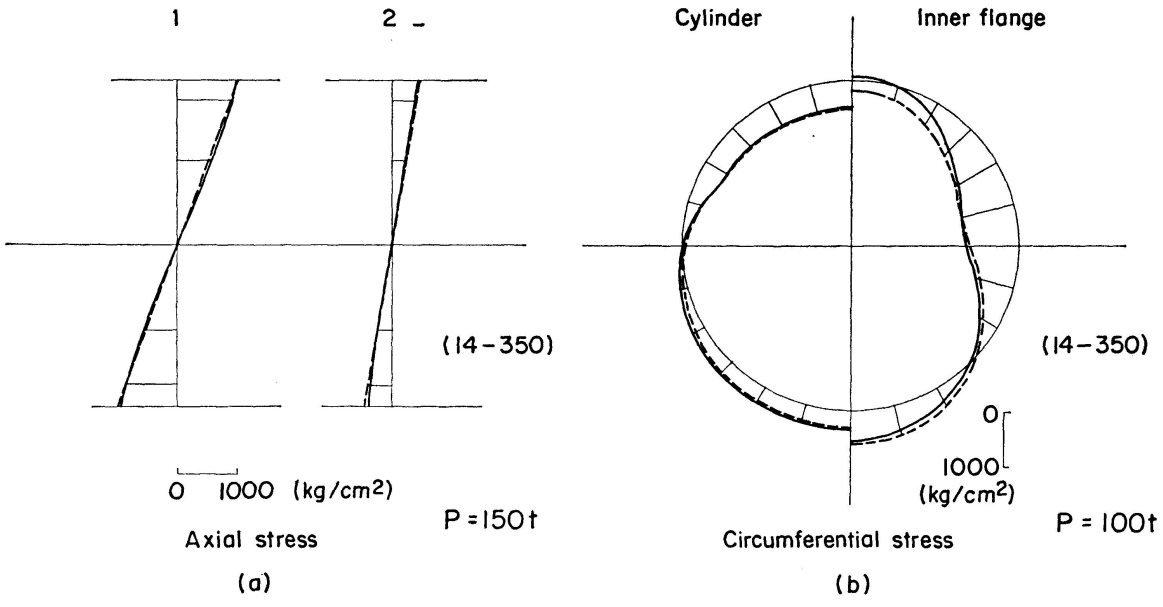

Fig. 44.

The interlocking type is nearly strong enough to satisfy M_p, while the butting type is a little short in strength but has relatively large rotating capacity.

A simplified form of bending test as shown in Fig. 43 was carried out for checking the stress of a cylinder and that of diaphragms.

According to the results of the test, the axial stress of the cylinder is close to the value calculated by the conventional beam theory as shown in Fig. 44 (a), and the circumferential stress of the cylinder and the stress of the diaphragms are nearly in coincidence with the above-mentioned calculated value as shown in Fig. 44 (b). How the diaphragms and the cylinder cooperate with each other was calculated from the axial distribution of the circumferential stress of the cylinder, the result of which is shown against R/t_p in Fig. 45. The value of b_3 calculated from Eq. (81) is fairly close to the measured value in thick-walled cylinders.

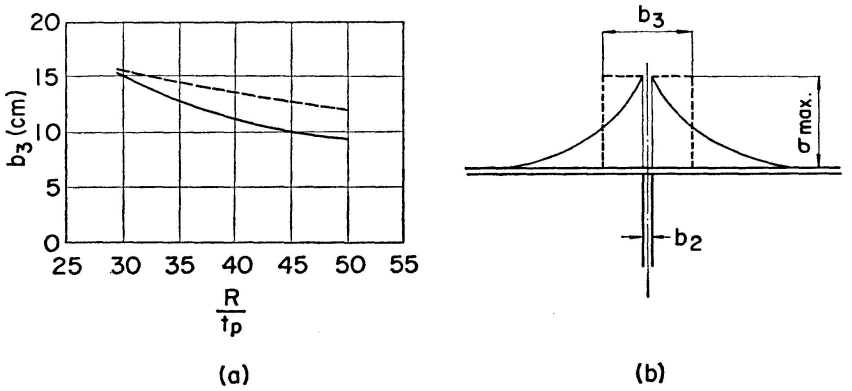

Fig. 45.

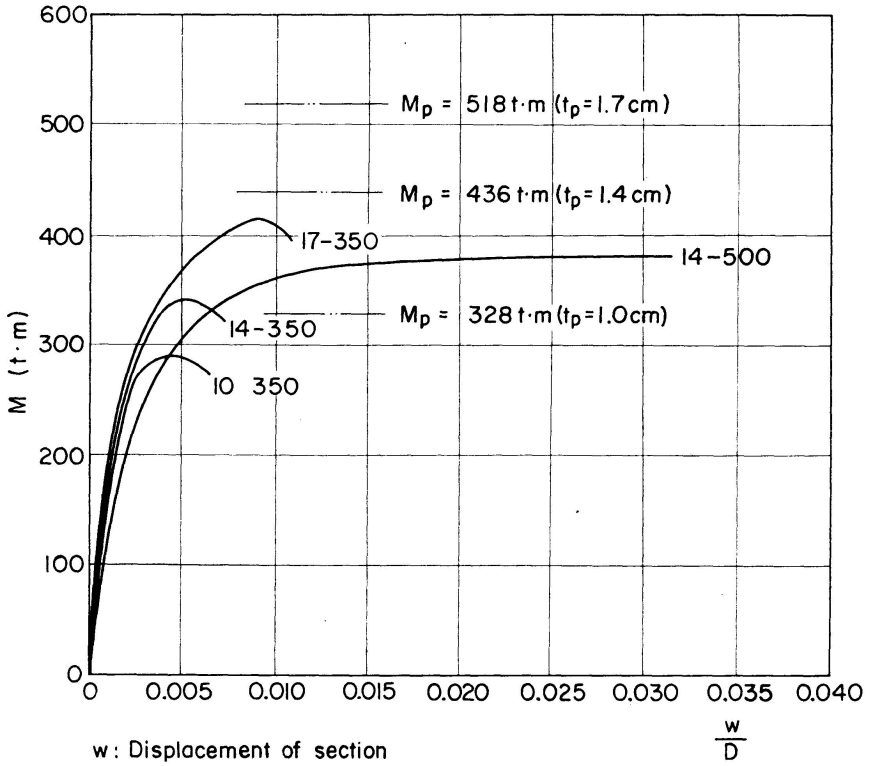

Fig. 46.

Diaphragms with a small value of a buckled in a rupture test, resulting in a premature lowering of yield strength (Fig. 46). It is necessary to pay due regard to the thickness of diaphragms with a small manhole radius. Even if diaphragms are provided with inner flanges, it is recommended that the thick-

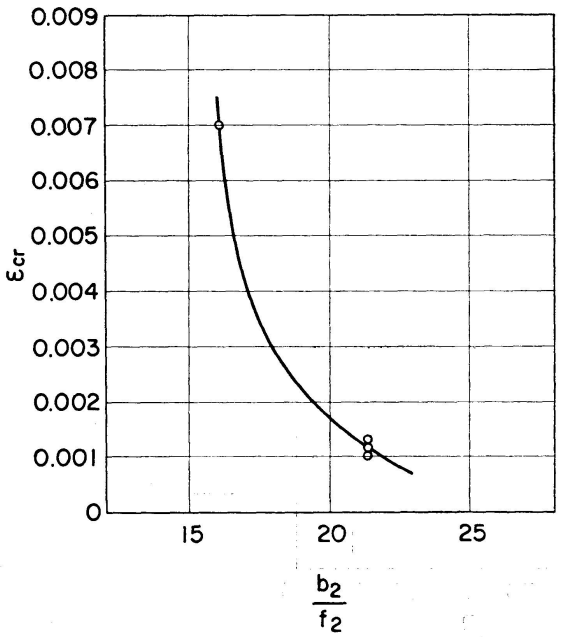

ε_{cr} : Limits of buckling strain

o Measured value

Fig. 47 (a).

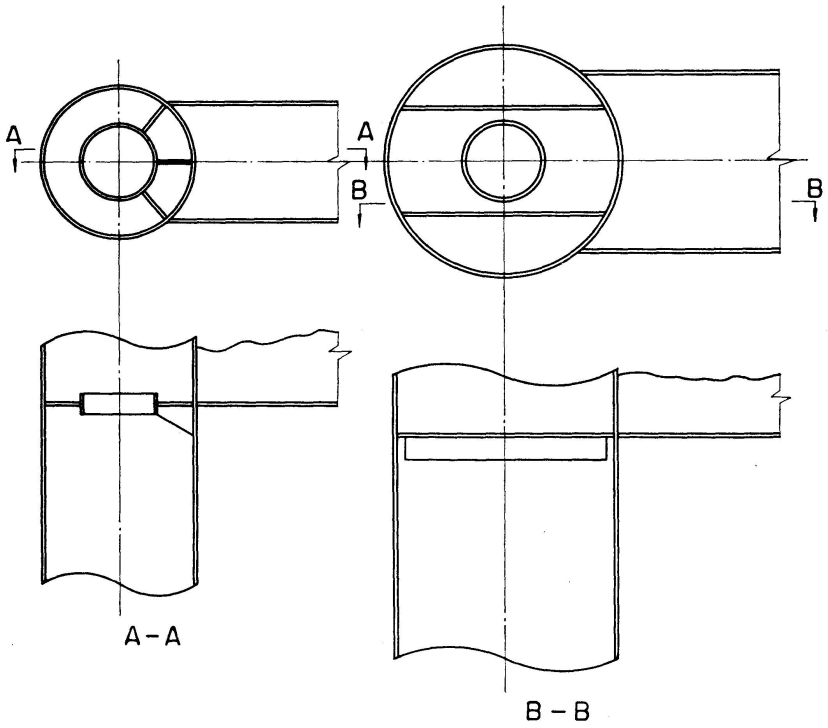

Fig. 47 (b).

ness of diaphragms be determined according to the conventional rule $b_2 \geqq \frac{f_2}{17}$ on the thickness of an intermediate stiffener or a free outstanding leg of a secondary member (Fig. 47 (a)). The stiffener shown in Fig. 47 (b) can be effectively used.

When the width of a beam is larger than the diameter of a cylindrical column, they are joined as shown in Fig. 48. They do not differ basically from the above-mentioned types. Fig. 49 shows a case applicable not only to force acting within the surface of rigid frame construction but to force acting outside its surface. It has been confirmed that, if diaphragms are arranged as shown in this figure and the oblique diaphragms extending from the cylinder to the beam flanges are made as thick as the cylinder wall and those extending in the axial direction of the beam are made as thick as the beam web in this case, it results in an appropriate value of the shearing stress in the knee joint and a fairly small value of the stress due to shear lag in the beam flanges.

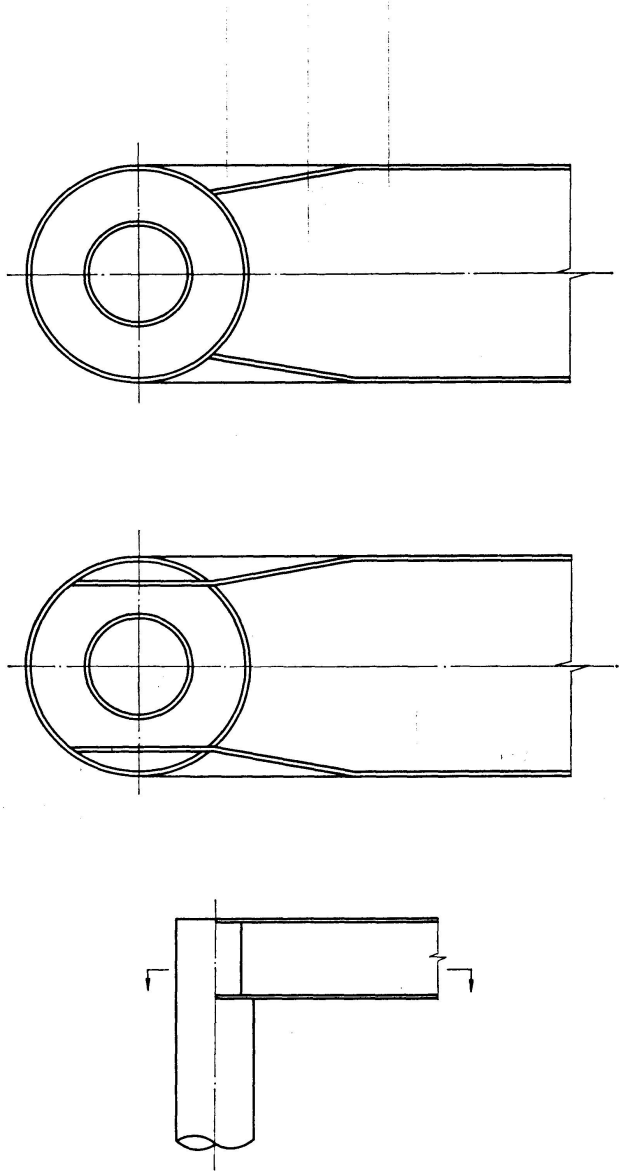

Fig. 48.

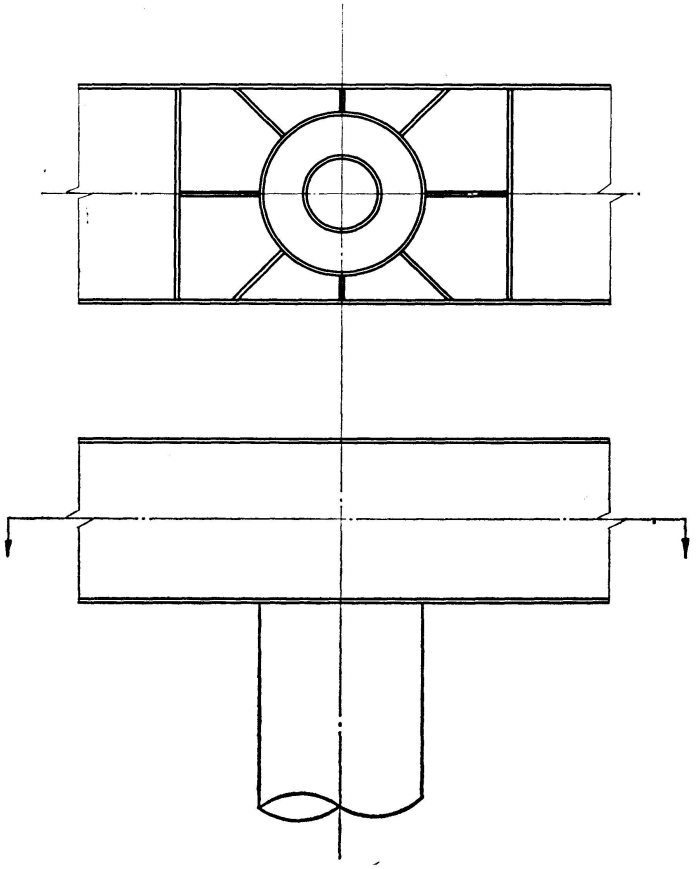

Fig. 49.

3. Circular Arc Knee Joint

When bending moment is applied to the rigid frame knee joint of box section shown in Fig. 50, stress exerted in the acute outer corner is very low. Therefore, the rigid frame knee joint is regarded as a bent tube of box section by assuming that the hatched part does not exist.

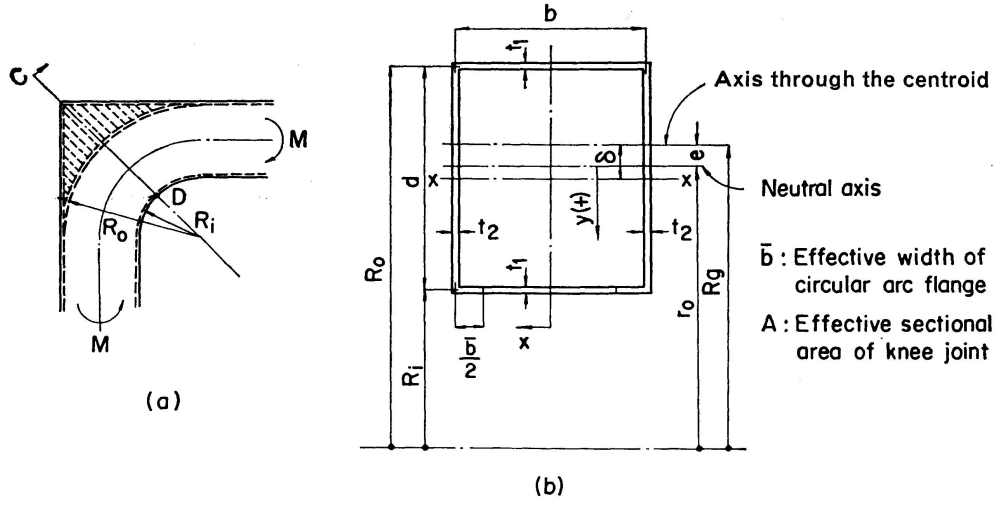

Fig. 50.

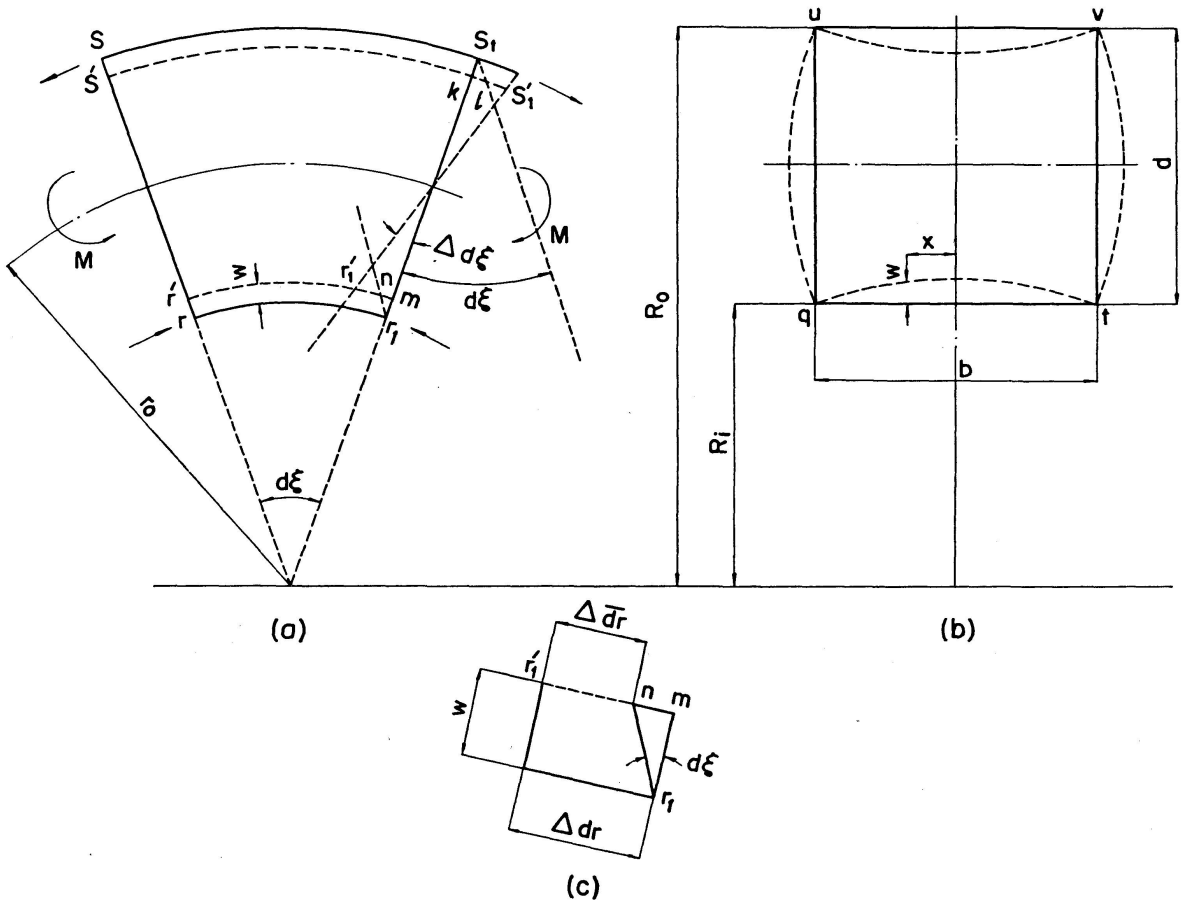

Fig. 51.

In the bent tube shown in Fig. 51, tensile force and compressive force are created in the outer and inner flanges, respectively, by bending moment. They give rise to resultant forces, each directed toward the neutral axis. These resultant forces cause the section to be deformed as shown in Fig. 51 (b). If it is assumed that the section of the bent tube continues to be a plane even after it is bent, the elongation (contraction) of the flange elements $S S_1$ ($r r_1$) at a distance of x from the symmetrical axis y is related not only to the increment $\Delta d\xi$ of the angle $d\xi$, but also to the displacement w in the radial direction of the section.

The strain in the lengthwise direction of the flange element $r r_1$ can be expressed in the form

$$\frac{\Delta \bar{dr}}{dr} = \frac{\Delta dr - w d\xi}{dr}. \tag{82}$$

And

$$\sigma_x = \frac{E}{1-\nu^2}\epsilon = \frac{E}{1-\nu^2}\left(\frac{\Delta dr}{dr} - w\frac{d\xi}{dr}\right) = \sigma_{max} - \frac{E}{1-\nu^2}\frac{w}{R_i}, \tag{83}$$

where σ_{max} is the flange stress right above the web, the value of which is taken at the center of the thickness of the flange.

The differential equation with respect to the displacement w of the flange plate can be written in the form

$$\frac{E t_1^3}{12(1-\nu^2)} \frac{d^4 w}{d x^4} = \sigma_x \frac{t_1}{R_i}. \tag{84}$$

By inserting Eq. (83) in Eq. (84) and putting $\sigma_{max} \frac{t_1}{R_i} = q'$ and $\frac{E}{1-\nu^2} \frac{t_1}{R_i^2} = k'$

$$\frac{E t_1^3}{12(1-\nu^2)} \frac{d^4 w}{d x^4} = q' - k' w. \tag{85}$$

Taking into account the symmetry to the y-axis and putting

$$\beta = \frac{b}{2} \sqrt[4]{\frac{3}{R_i^2 t_1^2}} \tag{86}$$

we obtain the solution in the form

$$w = \frac{q'}{k'} \left(1 - \boldsymbol{C}_1 \sin\frac{2\beta x}{b} \sinh\frac{2\beta x}{b} - \boldsymbol{C}_2 \cos\frac{2\beta x}{b} \cosh\frac{2\beta x}{b}\right). \tag{87}$$

Supposing that the webs uq and vt in a rigid frame having rigid joints u, v, t and q as shown in Fig. 51 (b) are deformed in circular arc form, the radius of curvature ρ of the web plates is expressed in the form

$$\left(\frac{d w}{d x}\right)_{x=\frac{b}{2}} = \frac{\frac{d}{2}}{\rho}. \tag{88}$$

On the other hand, the bending moment at the points q and t of the flange qt is defined as

$$\frac{E t_1^3}{12(1-\nu^2)} \left(\frac{d^2 w}{d x^2}\right)_{x=\frac{b}{2}} = \frac{E t_2^3}{12(1-\nu^2)} \frac{1}{\rho}.$$

From the above equation

$$\left(\frac{d w}{d x}\right)_{x=\frac{b}{2}} = \frac{d}{2} \left(\frac{t_1}{t_2}\right)^3 \left(\frac{d^2 w}{d x^2}\right)_{x=\frac{b}{2}}. \tag{89}$$

From Eq. (88) and $w_{x=b/2} = 0$, $\boldsymbol{C}_1$ and $\boldsymbol{C}_2$ can be derived in the form

$$\boldsymbol{C}_1 = \frac{\boldsymbol{s}\boldsymbol{C} - \boldsymbol{c}\boldsymbol{S} - \gamma \boldsymbol{s}\boldsymbol{S}}{\boldsymbol{c}\boldsymbol{s} + \boldsymbol{C}\boldsymbol{S} - \gamma(\boldsymbol{S}^2 + \boldsymbol{c}^2)}, \qquad \boldsymbol{C}_2 = \frac{\boldsymbol{s}\boldsymbol{C} + \boldsymbol{c}\boldsymbol{S} - \gamma \boldsymbol{c}\boldsymbol{C}}{\boldsymbol{c}\boldsymbol{s} + \boldsymbol{C}\boldsymbol{S} - \gamma(\boldsymbol{S}^2 + \boldsymbol{c}^2)}, \tag{90}$$

where

$$\gamma = 2\beta \frac{d}{b} \left(\frac{t_1}{t_2}\right)^3 \tag{91}$$

and

$$\sin\beta = \boldsymbol{s}, \quad \sinh\beta = \boldsymbol{S}, \quad \cos\beta = \boldsymbol{c} \quad \text{and} \quad \cosh\beta = \boldsymbol{C}. \tag{92}$$

Hence

$$\sigma_x = \sigma_{max} \left(\boldsymbol{C}_1 \sin\frac{2\beta x}{b} \sinh\frac{2\beta x}{b} + \boldsymbol{C}_2 \cos\frac{2\beta x}{b} \cosh\frac{2\beta x}{b}\right). \tag{93}$$

The flange force is defined as

$$2t_1\int_0^{\frac{b}{2}}\sigma_x\,dx = t_1\,\bar{b}\,\sigma_{max}. \tag{94}$$

From the above equation

$$\frac{\bar{b}}{b} = \frac{1}{2\beta}\frac{\gamma(\sin 2\beta+\sinh 2\beta)-2(-\cos 2\beta+\cosh 2\beta)}{\gamma(\cos 2\beta+\cosh 2\beta)-(\sin 2\beta+\sinh 2\beta)}. \tag{95}$$

If the value of β grows, for instance, $\beta \geqq 3$, Eq. (95) may be substituted by

$$\frac{\bar{b}}{b} = \frac{1}{2\beta}\frac{\gamma-2}{\gamma-1}. \tag{96}$$

$\frac{\bar{b}}{b}$ is morely related to the dimensions of the section and R_i.

If the value of $\bar{b}$ is made known, the maximum value of the flange stress can be calculated.

$$\sigma_{max} = \frac{M\left(r_0-R_i+\frac{t_1}{2}\right)}{A\,e\left(R_i-\frac{t_1}{2}\right)}. \tag{97}$$

The distance r_0 between the neutral axis and the center of curvature can be written in the form

$$r_0 = \frac{A}{(b+t_2)\log_e\frac{R_0+\frac{t_1}{2}}{R_0-\frac{t_1}{2}}+2t_2\log_e\frac{R_0-\frac{t_1}{2}}{R_i+\frac{t_1}{2}}+(\bar{b}+t_2)\log_e\frac{R_i+\frac{t_1}{2}}{R_i-\frac{t_1}{2}}}. \tag{98}$$

Results of Experiment

An experiment was carried out to prove that the above-mentioned presumptive calculations were correct from a practical point of view.

The shape and dimensions of the specimen used in the experiment is shown in Fig. 52. The axial distribution of the axial stress of the circular arc flange is shown in Fig. 53 and 54.

According to the result of the experiment, the stress distribution of the axial stress of the circular arc flange at the point D is concentrated in the proximity of the web. The stress distribution along the circular arc is found not to change greatly in the circular arc. It will be seen that the above-mentioned calculations provide values close to the measured values. These calculations were made on the assumption that the effective width of the outer flange is equal to b or it is effective over its total width.

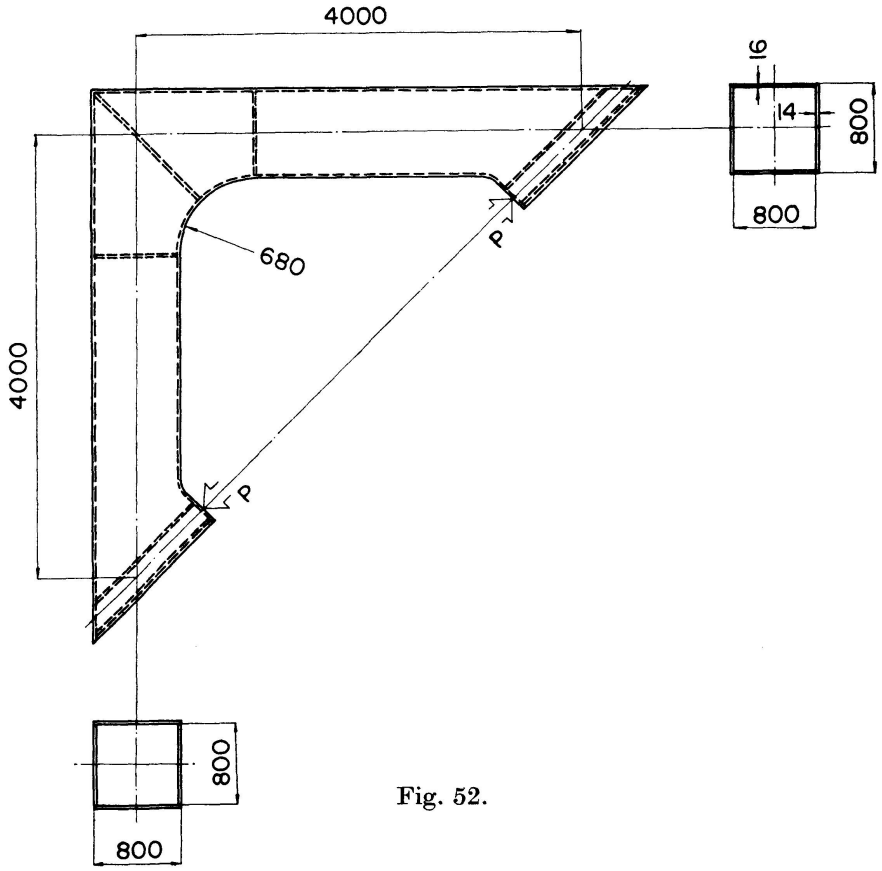

Fig. 52.

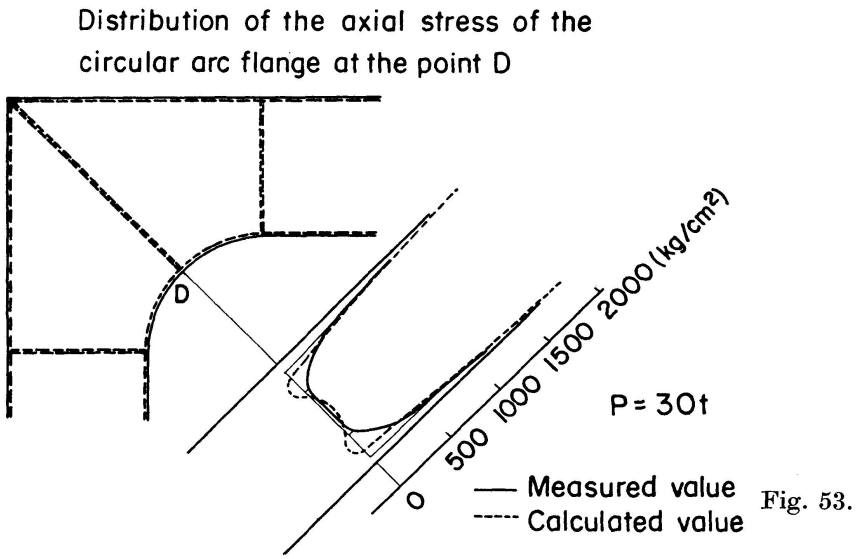

Fig. 53.

An $M-\Delta i$ curve is shown in Fig. 55. The load is of open type. According to this, it will be seen that M_p can be reached easily. In this case, however, careful attention must be paid to great stress concentration arising in the proximity of the flange web because the section is warped in the proximity of the circular arc flange of the knee joint. For this reason, the oblique reinforcements shown in Fig. 56 may serve effectively.

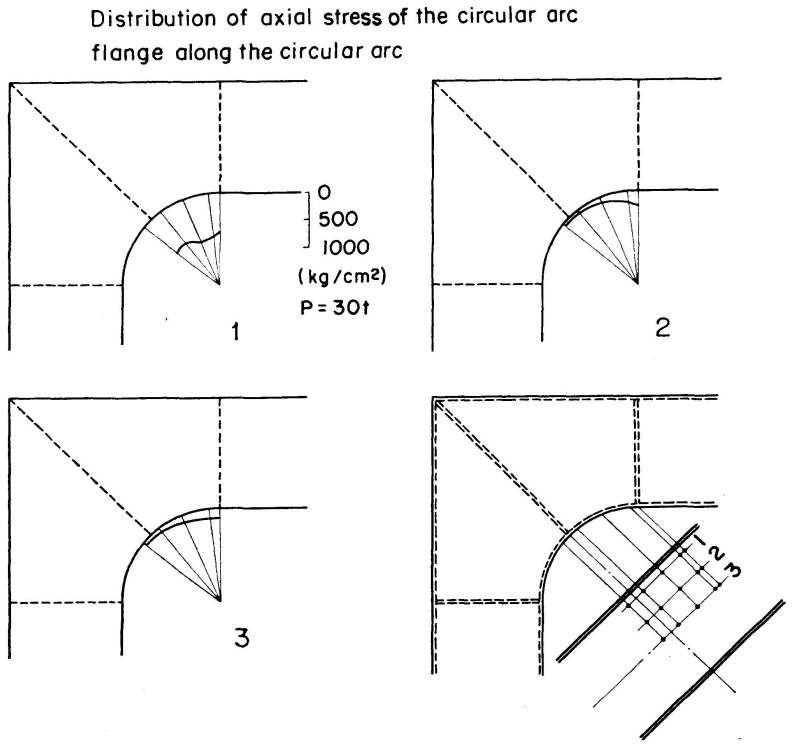

Fig. 54.

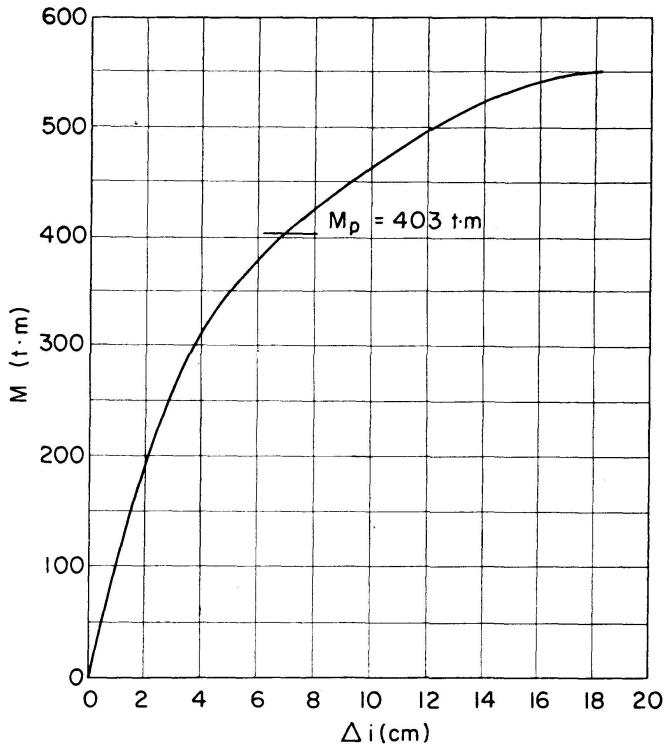

Fig. 55.

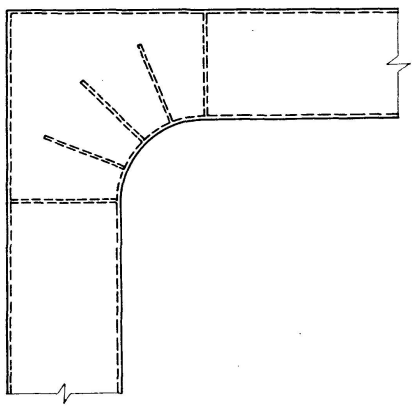

Fig. 56.

Conclusion

In this report are presented some proposals for the calculation of stress at rigid frame knee joints in which beams with box section are used, and the

results of examination of the proposals through experiments have been described.

It is suggested that conventional methods of calculation made on the assumption that shearing stress is uniformly distributed in the web of straight rectangular knee joints should be corrected. It is also suggested that the stress due to shear lag obtained by model calculation must be considered with respect to flange stress. Diagrams used for estimating the stress due to shear lag are made available for this purpose. At the same time, it is pointed out that these ideas are applicable to such types as straight haunch type and circular arc type straight flanges. When the application of plastic design is considered, it is necessary to pay due regard to the thickness of knee joints, because, generally in such knee joints, the total plastic moment of column or beam is apt to be lowered by shearing stress. As large stress concentration will occur near the inside of knee joints, it is necessary to render the total strength of flange to the joints to be welded. The effect of inserted web on shearing stress in knee joints, when a cylindrical column is used, has been detailed in this paper. The necessity of paying due regard to shear lag is also discussed in considering the stress to beam flange as in the case of straight rectangular type. As fairly large stress is generated in the inner flange of diaphragm, or as the diaphragm possibly buckles at too early a stage, depending on its dimension, the method of calculation of the diaphragm stress and the limitation of the thickness of diaphragm were called to particular attention.

As for the circular arc knee joint, this report shows the method of calculation of the circular arc flanges, in which the warping of web and flange of knee joint is taken into consideration. In this case, section arrangement and the thickness of the plate must be determined carefully because fairly large stress concentration is observed in the proximity of the web of the circular arc flange. According to the results of experiments with the above-mentioned types, the calculated values generally come in coincidence with the values obtained by the experiments.

These are the points which must be considered in designing knee joints of welded construction. While some more problems are yet to be examined as to stress concentration at the inner point in the knee joints or stress disturbance in the proximity of the inner point in the web, the methods of calculation proposed herein are believed to provide some references for solving these problems.

Reference Materials

1. T. Okumura: Problems Involved in Design and Working of Thin-Walled Section. Publication of Recent Problems in Structural Engineering, Japan Society of Civil Engineers, August 1965.
2. L. S. Beedle, A. A. Topractsoglou, and B. G. Johnston: Connections for Welded Continuous Portal Frames, Welding Journal, 30 (7), 30 (8) and 31 (11), 1951 and 1952.

3. D. T. WRIGHT: The Design of Knee Joints for Rigid Steel Frames. British Welding Journal, B.W.R.A., April 1954.
4. I. LYSE, and W. E. BLACK: An Investigation of Steel Rigid Frames. Trans. A.S.C.E., 107–186, 1942.
5. I. M. YUILLE: Shear Lag in Stiffened Plating. Originally published for Written Discussion, Transactions of the Institute of Naval Architects, Vol. 97.
6. T. OKUMURA, K. MAEDA, and N. ISHIZAWA: Knee Joints of Rigid Frames in These Days. Journal of the Japan Society of Civil Engineers, November 1964.
7. Valves Gates and Steel Conduits, Chapter 2, Department of Interiors Bureau of Reclamation, U.S.A.
8. S. TIMOSHENKO: Bending Stress in Curved Tubes of Rectangular Cross-Section. A.S.M.E., Vol. 45, p. 135, 1923.
9. F. BLEICH: Stahlhochbauten, Bd. 2.
10. KAYSER und HERZOG: Versuche zur Klärung des Spannungsverlaufes in Rahmenecken. Der Stahlbau, Jahrgang 12, Heft 2, 20. Jan. 1939.
11. C. G. ANDERSON: Flexural Stresses in Curved Beam of I – and Box-Sections. Proceedings Applied Mechanics, The Institution of Mechanical Engineers, London, Vol. 163, 1950.
12. I. OHNO: Formulas for Design of Corner of Steel Rigid Frame. Journal of The Japan Society of Civil Engineers, Sept. 1952.
13. T. OKUMURA, M. ITO, Y. NISHINO, K. MAEDA, N. ISHIZAWA: Connections on Rigid Frame Steel Structures Recently Adopted in Japan. Proceedings of the Conference on Experimental Methods of Investigating Stress and Strain in Structures, Praha, October 1965.
14. T. OKUMURA, N. ISHIZAWA: The Design of Knee Joints for Rigid Steel Frames with Thin Walled Section. Proceedings of The Japan Society of Civil Engineers, No. 153, May 1968.

Summary

The authors present some proposals in this paper regarding calculation of stress at knee joints of rigid frame construction, and confirm the applicability through several experiments. A few types of knee joints, such as straight rectangular, straight haunch and circular arc haunch, have been investigated.

One of the features of this report is that the stress due to shear lag is taken into consideration with respect to flange stress in knee joints formed by welded beam and column of box section. The stress due to shear lag can be calculated by means of model, and diagrams are used for estimation of the stress. Not only columns with box section but cylindrical columns are discussed in this paper.

Résumé

Le présent article contient quelques propositions pour le calcul des nœuds de cadres rigides et confirme son application par divers essais. On a examiné plusieurs types de nœuds: forme rectangulaire, polygonale et en arc de cercle.

Ce qui caractérise cet article est le fait que nous avons considéré l'influence

de la déformation du cisaillement sur les contraintes des semelles. Cette influence peut être obtenue à partir de modèles mathématiques et de graphiques. En outre, on examine le cas des colonnes cylindriques.

Zusammenfassung

Die Verfasser unterbreiten in diesem Beitrag einige Vorschläge zur Spannungsberechnung an Rahmenecken und bestätigen die Anwendbarkeit durch verschiedene Versuche. Etliche Typen von Rahmenecken, wie rechtwinklige, polygonale und kreisförmige werden untersucht.

Eines der Merkmale im vorliegenden Aufsatz äußert sich darin, daß die Spannungsänderungen in den Flanschen infolge der Schubverformung in Betracht gezogen werden. Der Einfluß der Schubverformung kann anhand von Modellen ermittelt und zur Schätzung der Spannung können Diagramme benutzt werden. In dieser Arbeit werden nicht allein Stützen mit kastenförmigem Querschnitt, sondern auch zylindrische Stützen behandelt.